A Human-Portable Mass Flux Method for Methane Emissions Quantification: Controlled Release Testing Performance Evaluation

Coleman Vollrath, Thomas Barchyn, Abbey Munn, Clay Wearmouth, and Chris Hugenholtz

Department of Geography, University of Calgary, Calgary, Alberta, T2N 1N4, Canada

5   *Correspondence to*: Coleman Vollrath (coleman.vollrath1@ucalgary.ca)

Abstract. Quantifying methane (CH_4) emissions from anthropogenic sources is essential for compliance, inventory, and verification efforts. One established mass balance approach is the mobile flux plane method, in which emissions can be estimated from measurements of CH_4 at various heights. Most traditional applications require either a drone or aircraft, both of which can be expensive, or limiting to deploy in all situations. To broaden applicability and improve practicality, we adapted

10   the flux plane method using a long telescoping pole and backpack-mounted CH_4 sensor. We explored accuracy through 44 controlled release experiments (0.2–5.6 kg CH_4/h) from a 2.4 m stack. Measurements were taken at 6 heights (0.8–5.6 m) by walking transects 10–30 m downwind. The data yielded a mean relative error of -10.1%, with 68% of estimates within ±38.3% of true values. Results are comparable to drone-based methods. We also tested an optimized Gaussian plume model using partial vertical profiles to address issues where the pole could not measure the top of the plume. This approach was slightly

15   less precise than the flux plane method and had less bias. Overall, results show that multi-level, telescoping pole-based CH_4 measurements combined with flux plane or Gaussian models can (i) quantify emissions from elevated sources in a logistically practical manner with results comparable to other widely used mobile quantification methods, and (ii) quantify sources emitting CH_4 at low rates owing to the close-range capability of the method, complementing other mobile methods such as vehicle-based systems, aircraft, and satellites that generally measure higher-emitting sources.

1 Introduction

20   Methods to quantify anthropogenic methane (CH_4) emissions have become increasingly important recently as efforts to reduce emissions have expanded. Abating CH_4 emissions is an effective method to mitigate global warming as CH_4 is a potent and short-lived greenhouse gas. The bulk of this method development has occurred within the oil and gas industry, driven by: (i) recognition that the oil and gas industry—a large emitter of CH_4—is emitting more than previously estimated (Howarth et al.,

25   2011; Alvarez et al., 2018); (ii) cost-effective and high deployment readiness of mitigations (Ocko et al., 2021); (iii) regulations (e.g., EPA, 2023; European Commission, 2022; Government of Canada, 2023); and (iv) voluntary commitments by governments and the oil and gas industry to reduce CH_4 emissions or credibly demonstrate the climate performance of natural gas. These factors and developments, alongside rapid advancements and innovation in CH_4 sensor technology, have nurtured

the development of an expansive toolkit of quantification methods covering a variety of sources and rates in the oil and gas
30   industry at different spatial and temporal scales (Vollrath et al., 2024).

Mass balance is a quantification method that uses directly measured CH_4 concentration and local wind measurements to evaluate the integrated CH_4 flux over a measurement plane or path (Karion et al., 2013; Conley et al., 2017; Corbett and Smith, 2022; Mohammadloo et al., 2025). The typical approach involves measuring CH_4 at various elevations (from ground level to above the plume), transecting the plume in a crosswind manner. With these data, the full cross-section of the plume
35   can be approximated, and total flux can be estimated by multiplying the approximated concentration data by advection (wind speed) and integrating across the full cross-section. CH_4 can also be measured at a single elevation, typically in very far downwind applications such as basin-scale quantifications (Karion et al., 2013; Peischl et al., 2018), and careful assumptions made about the atmospheric boundary layer to assume the plume is homogenously mixed vertically.

Provided CH_4 measurements can be obtained across the full extent of the plume, mass balance methods have major
40   advantages over atmospheric dispersion modeling. Atmospheric dispersion modeling often requires assumptions about atmospheric behaviour and in most cases is led by knowledge of the source location and characteristics. For large area sources, or complex situations with many sources with unknown rates and locations, traditional dispersion modeling can be extremely difficult. Difficulties with traditional dispersion models are exacerbated at close ranges and in situations where dispersion diverges significantly from theory and plumes are variable in form (Caulton et al., 2018).

45   The dominating practical challenge associated with mass balance methods is obtaining direct measurements of CH_4 across the full elevation of the plume. Plumes tend to vertically and laterally expand with downwind distance, becoming better mixed and extending higher into the atmosphere. The combination of this lateral and vertical expansion creates application specific constraints. Lateral dispersion and the desired spatial scale of measurement strongly affect where measurements must be taken. For example, measurement of individual oil and gas sites often cannot be meaningfully achieved tens of kilometers
50   downwind, as plumes from adjacent sites mix, introducing significant error into attribution and effectively limiting the spatial scale of the mass balance measurement. To measure individual equipment on oil and gas sites, data must usually be collected within tens of meters downwind. Plumes at tens of kms downwind can extend far above the surface, but close range plumes are much closer to the ground. Further complicating this, some release points of interest are elevated (e.g., flares, tank tops, etc.), meaning the plume disperses from the release point both up and down within the atmosphere. These application
55   constraints coupled with the typical geometry of plumes have led workers to use a broad diversity of platforms to address various spatial scales of measurement:

(i)   Drones are highly suitable for measurements of equipment, typically at the tens to hundreds of m downwind range, enabling measurements of CH_4 at hundreds of m elevation and close to the ground (e.g., Nathan et al.,
60   2015; Tullos et al., 2021; Corbett and Smith, 2022; Dooley et al., 2024). This noted, drones differ. Fixed-wing drones often are limited in their ability to fly close to the ground compared to quadrotor drones (e.g., Nathan et

al., 2015; Barchyn et al., 2017), limiting application to larger spatial scales where the bulk of the plume disperses upwards and the lack of measurements close to the ground are less limiting.

(ii)   Aircraft are best suited for measurements of larger facilities or groups of wells and facilities kms downwind
65   (Conley et al., 2016; 2017; Lavoie et al., 2017; Li et al., 2024; Maazallahi et al., 2025). Similar to fixed-wing drones, aircraft cannot fly low. Other approaches involving the use of aircraft in extremely far downwind applications are noted (e.g., Karion et al., 2013; Peischl et al., 2018) but are largely inapplicable for finer spatial scales.

(iii)   Ground measurements (by foot, truck, or similar) are limited to site or finer spatial scales (measured tens to
70   hundreds of m downwind). Ground access only allows measurement of the bottom portion of the plume. Efforts to get around this limitation have taken the form of vertical masts attached to vehicles (e.g., Thoma et al., 2015; Rella et al., 2015), but there are clear practical limits on the height of poles on vehicles associated with overhead obstacles on roads.

75   In the situation where only a portion of the vertical extent of the plume can be measured, a strategy is to augment the mass balance method with traditional plume models, creating a hybrid model that is more practical, but potentially carries larger error. Rella et al. (2015) used a Gaussian plume model to approximate unmeasured CH_4 above the reach of their vehicle-based pole. Similar issues occur with aircraft which face the opposite problem of being unable to measure the plume close to the ground. Traditional plume modeling (e.g., Caulton et al., 2018) is the endmember of this continuum where the vertical
80   distribution of CH_4 is entirely modeled and measurements only exist near ground level.

The oil and gas industry has particular need for close-range methods that can accurately measure emissions from individual equipment on sites. Particularly problematic are emissions from high tank vents, flare stacks, or other elevated sources. Mass balance methods are well suited for these applications because close-range plumes tend to be poorly mixed and rarely conform to traditional plume model assumptions (Caulton et al., 2018), and there is a unique difficulty associated with
85   performing measurements at close enough distances downwind (to accurately attribute emissions to individual pieces of equipment) but at sufficient elevations to capture the full plume (to reduce the need for models to predict unmeasured portions of the plume).

The dominant approach for these close range measurements is mounting a sensor on drones which are then flown tens of m downwind. CH_4 emissions can be quantified using the flux plane method—an established mass balance approach—which
90   involves projecting the measurements collected downwind of the source onto a two-dimensional plane oriented perpendicular to the wind direction (Nathan et al., 2015; Corbett and Smith, 2022). The plane is discretized into a grid across which the measurements are interpolated. This simulates a crosswind slice of the plume smoothed over time and space. Estimates of background CH_4 concentration and the local wind speed are then used to estimate the CH_4 flux passing through each discrete grid cell. Finally, the fluxes are integrated across the grid to estimate an emissions rate. Tests using quadrotor drones and the
95   flux plane method exhibited a mean relative error of ±36.7% in non-zero controlled release experiments simulating a point

source emitter (Corbett and Smith, 2022). Recent controlled release tests from within a closed landfill in Ontario, Canada suggest similar performance for area source quantification—mean errors of ±34.7% and ±62% were reported for two study participants using quadrotor drones and the flux plane method, respectively, across the series of tests (Hossian et al., 2024). The ability of quadrotor drones to conduct vertical and close-to-source flights provides key advantages for emission quantification with the flux plane method. However, drones cannot be flown everywhere, and the cost and sophistication of the miniaturized sensors remains a barrier to widespread application. Alternative or complementary methods that are simple, reproducible, easy to deploy, and accessible—while ensuring unbiased and accurate estimates—are warranted.

Here, to address the logistical issues associated with drones and advance methodologies associated with the flux plane method, we explore the use of a long pole, walked downwind of sources at various heights. This approach shows promise as it is logistically simple, comparatively safe, potentially low cost, and accessible to many researchers. Similar to how drones cannot be flown everywhere, it should be emphasized that the walking measurements demonstrated in this study also cannot be performed everywhere—access, terrain, source characteristics, safety, and meteorological conditions can create constraints for the method. We tested the full method in a series of controlled release experiments. We evaluated error to assess quantification accuracy and understand sources of error. To address situations where the pole cannot reach the top of the plume, we developed and tested a supplementary method that uses a customized forward Gaussian plume model. The results qualify the performance of the method for broader use in CH_4 emissions quantification.

2 Methodology

2.1 Test facility and release setup

We performed controlled releases of CH_4 on the 11, 12 of June and 6 August 2024 at the Carbon Management Canada (CMC) research site located approximately 20 km southwest of Brooks, Alberta (50.450510°, -112.120637°). We released natural gas from a compressed natural gas (CNG) trailer through a ~2.4 m tall release stack positioned in a large field. The terrain is flat with short- to medium-length grasses (0.2 m to 0.5 m) (see Fig 1). Gas was preliminarily regulated, then flowed to an ambient heat exchanger, which brought the temperature of the gas closer to the ambient atmosphere. An Alicat Scientific mass flow controller (MCR 2000SLPM-D) was then used to set and maintain release rates. The specification accuracy of the flow controller is: ± (0.8% of reading + 0.2% of full scale). During installation, release components were inspected using olfactory detection, personal multi-gas monitors, and an optical gas imaging (OGI) camera to identify any leaks. Wind speed and direction were measured with an RM Young 81000 3D sonic anemometer and data logger at 10 Hz a few meters away from the release stack at a height of 2.2 m. The locations of the release stack and anemometer were recorded with a survey-grade GPS.
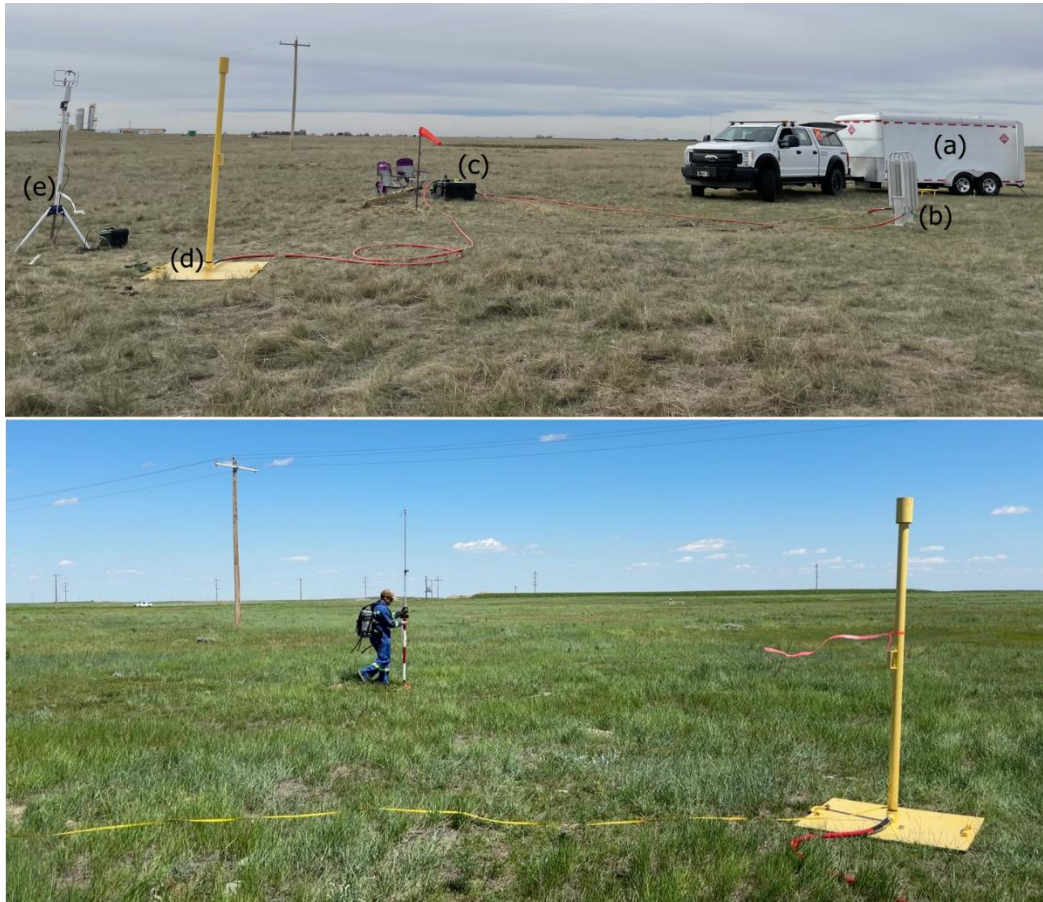
Figure 1. Top panel—Controlled release setup. (a) CNG trailer with tanks. (b) ambient heat exchanger. (c) flow controller. (d) release stack. (e) anemometer. Bottom panel—the pole-based measurement system in operation during a controlled release test on 12 June 2024. The operator carried a CH₄ sensor in a backpack harness and a long length of hose was run from the sensor's inlet to the end of the pole where air was drawn in. Photo credits Zhenyu Xing and Chris Hugenholtz.

Non-target sources of potential CH_4 emissions were screened using the University of Calgary's PoMELO vehicle system (Barchyn and Hugenholtz, 2020; 2022) to confirm that methane from unexpected upwind sources were not present during testing.

Gas samples were extracted from the CNG tanks to determine the average CH_4 content to correct the measured rates from bulk gas to CH_4. Samples were retrieved by creating a pneumatic trap in a bucket of water, which used gas flow to fill an evacuated syringe and limit contamination from air. Samples were transferred to septa bottles for gas chromatography analysis. Additional details are provided in the Supplemental Material (S1). Samples indicated released gas had an average CH_4 content of 90.5%.

2.2 Measurement kit and instrumentation

The pole-based measurement system developed for this test campaign consisted of a LI-COR 7810 (LI-7810) trace gas analyzer in a backpack harness, an iPhone 14 Pro with Avenza Maps for GPS, a ~4.6 m SECO extendable aluminum survey pole, ~5.5 m of Teflon hosing, and a fanny pack (Fig 1 bottom panel). The hosing was connected to the LI-7810 inlet with a Swagelok fitting and run to the top of the pole, such that the height of the hose inlet changed as the pole was repositioned or extended. Although the analyzer was near ground level, the sample inlet was located at the top of the pole. The maximum practical height of CH_4 measurement was 5.6 m, the minimum height could be within cms of the ground. The iPhone 14 Pro was mounted to the pole using a bicycle cellphone mount such that the pole operator could view CH_4 mixing ratios measured by the LI-7810 in real-time and to record GPS location.

The LI-7810 measures CH_4, CO_2, and H_2O vapor at 1 Hz; it has a measurable range of 0 to 100 ppm CH_4 with a precision (σ) of 0.6 ppb at 2 ppm over 1 s (LI-COR, 2025). The LI-7810 pulls air into its sensor cavity through an internal pump at a rate of 0.25 L/min. Air transit from the end of the hose to sampler creates a time delay, which was measured using two methods. First, a small volume of bump gas (2.5% CH_4) was released near the end of the tubing with the LI-7810 running. Second, we preformed a "CO_2 breath test," where a participant exhaled near the end of the hosing. A stopwatch was started upon the participant releasing the gas or exhaling and stopped when the LI-7810 detected enhanced CH_4 or CO_2. Both methods produced comparable results (16.4 s vs. 16.1 s) upon averaging a series of five tests. To minimize interpolation in subsequent time-matching (and associated data smoothing), we used a round number 16 s time offset.

The iPhone 14 Pro is equipped with a precision dual-frequency GPS. We monitored GPS accuracy and estimated the average horizontal spatial accuracy of the iPhone's GPS to be ~3 m. Note that there is no sky obstruction at the CMC test facility to limit or vary position accuracy throughout experiments. Location data were logged every 1 s to match the frequency of the LI-7810. Measurement height of the data was populated in post-processing (see details in Sect. 2.5.) and is expressed as heights relative to the surface.

2.3 CH_4 release rates

We performed a total of 44 controlled release experiments over 11, 12 June and 6 August 2024. Release rates varied between 0.2 to 5.6 kg CH_4/h. This range was chosen such that the testing covered the anticipated CH_4 emissions rates of a variety of oil and gas related sources, including natural gas distribution facilities (Lamb et al., 2015) and lower-emitting oil and gas production sites (e.g., see Fig 8a in Vollrath et al., 2024). The release rates tested in this study were not representative of higher emitting oil and gas production sites. We performed 2 replicates of the following rates 1.8 kg/h, 2.6 kg/h, and 3.3 kg/h. Replicates were performed on different days to vary atmospheric conditions. Two experiments at different downwind distances—either 10 m and 20 m or 15 m and 30 m—were performed for each release. See Table S1 for full details.

2.4 Data collection procedure

Measurements were made in an arc around the release stack. This ensured that plumes were fully transected during each pass while minimizing the need to "chase" the plume around (i.e., walk further due to plume meander, as may be required with straight-line approaches) and walking distance. Additionally, performing measurements along an arc enabled standardization of the measurement distance and exploring the potential correlation between measurement distance and quantification error. We used a 50 m tape to flag distances of 10 m, 15 m, 20 m, and 30 m. The operator walked the flagged routes with the LI-7810 and telescoping pole to transect the plume. For each experiment, the release rate was set and surveys commenced after a ~3 minute delay to allow plume development. All surveys involved measurements both in the plume and in adjacent, non-plume atmosphere. Measurements outside of the plume are necessary to approximate the background CH_4 concentration.

During surveys, the operator oriented the telescoping pole such that the inlet of the tubing was facing the release stack. CH_4 mixing ratios were monitored in real-time (with olfactory detection of mercaptan, CH_3SH) to confirm the plume had been transected successfully. After passing the plume, the operator generally continued to the endpoint of the arc to ensure the plume was fully captured horizontally and that background CH_4 was sampled. In some cases, the operator walked further than or stopped short of the ends of the pre-marked routes depending on where the plume intersected the arc to improve sampling efficiency or collect additional data to use in estimating background CH_4. The operator then reversed the transect. This procedure was performed for a total of six measurement heights, yielding two transects (there and back) for each height (i.e., 12 plume passes). Figure 2a shows the arc transect pattern for experiments at 15 m and 30 m downwind of the stack during a release of 2.4 kg CH_4/h, and Figs 2b and 2c show measured CH_4 mixing ratios as a function of increasing measurement height during these experiments.
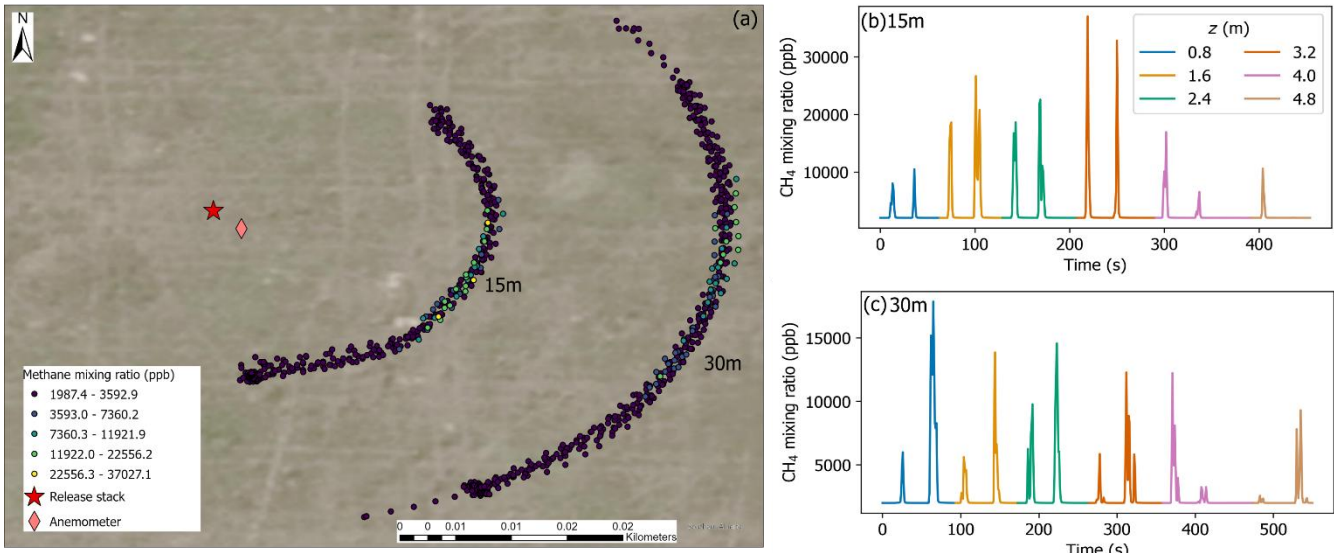
Figure 2. (a) arc transects walked with the backpack-mounted CH_4 sensor and telescoping pole at 15 m and 30 m downwind of the controlled release stack during a release of 2.4 kg CH_4/h on 12 June 2024. Circle colors correspond to CH_4 mixing ratios in the legend. (b) and (c) CH_4 mixing ratios by measurement height during the experiments at 15m and 30m downwind distances. The legend in (b) corresponds to measurement height by color in (b) and (c). Each group of two peaks corresponds to two passes of the plume at a single measurement level. Low or no visible enhancements towards the end of the experiments at higher measurement heights suggests the highest measurement heights captured the vertical extent of the plume.

The measurement heights varied slightly between experiments. On 11 June 2024 the measurement range was ~0.8 m to 4.7 m with ~0.8 m spacing between the six measurement levels. On 12 June 2024 experiments were similar but had a slightly higher top measurement level of 4.8 m due to some improvements to methods to support the pole, facilitating a higher top height. On 6 August 2024, the top height was 5.6 m with approximately 1 m spacing between measurement levels. The release stack height of ~2.4 m suggested that the maximum height of the pole measurements was 2 to 2.3 times higher.

2.5 Data preprocessing

Data preprocessing began by correcting any measured time offsets between the LI-7810 and GPS data. Then, the static correction (16 s) for delay associated with air transit was applied. The GPS and LI-7810 data were fused, joining by time. Measurement height was attributed to the data based on the start and stop times of the measurements at each height. The angles and distances between the release stack and all measurement points were calculated. The spatial locations of the points (x, y) were plotted in cartesian coordinates where the release stack was located at (0, 0). Finally, we visually examined the plotted measurement locations, trimming the data in some cases where the vast majority of measurements were in non-plume

atmosphere. This enabled defining flux planes that were better fit to the scales of individual plumes, while still including non-plume data for background CH_4 estimation.

2.6 Flux plane method

2.6.1 Procedure to define the plane and project and interpolate the data

The flux plane method involves projecting the downwind CH_4 measurements onto a two-dimensional plane oriented perpendicular to the wind direction. CH_4 molecules are assumed to be advected through the plane by the wind. This simulates a crosswind slice of the plume and addresses potential issues with "off-axis" CH_4 measurements, which could distort the plume's shape and thus affect the estimated flux. There is, however, limited guidance in the research literature on determining the horizontal extent of the flux plane (Nathan et al., 2015; Rella et al., 2015; Corbett and Smith, 2022). Therefore, after preprocessing the data, we defined the horizontal extent of our flux plane as the distance between the maximum and minimum (x, y) measurement locations (orange points Fig 3), such that relative to the wind direction, the flux plane is initially situated in front of most measurement points downwind (blue line in Fig 3). We then adjusted the position of the flux plane using the average of the measurement locations (yellow diamond Fig 3) as the plane's (black line Fig 3) midpoint, as this minimizes the projection distance for the points onto the two-dimensional plane (Nathan et al., 2015). Higher data density at the starting point of the arc transects—due to the operator adjusting the height of the pole at this location after each set of two consecutive plume passes—may have influenced the point's location and is an area for method improvement. We rotated the plane to be perpendicular (green line Fig 3) to the reference wind direction/plume centerline, which we defined as the angle between the release stack and the peak CH_4 location in each experiment (Caulton et al., 2018).
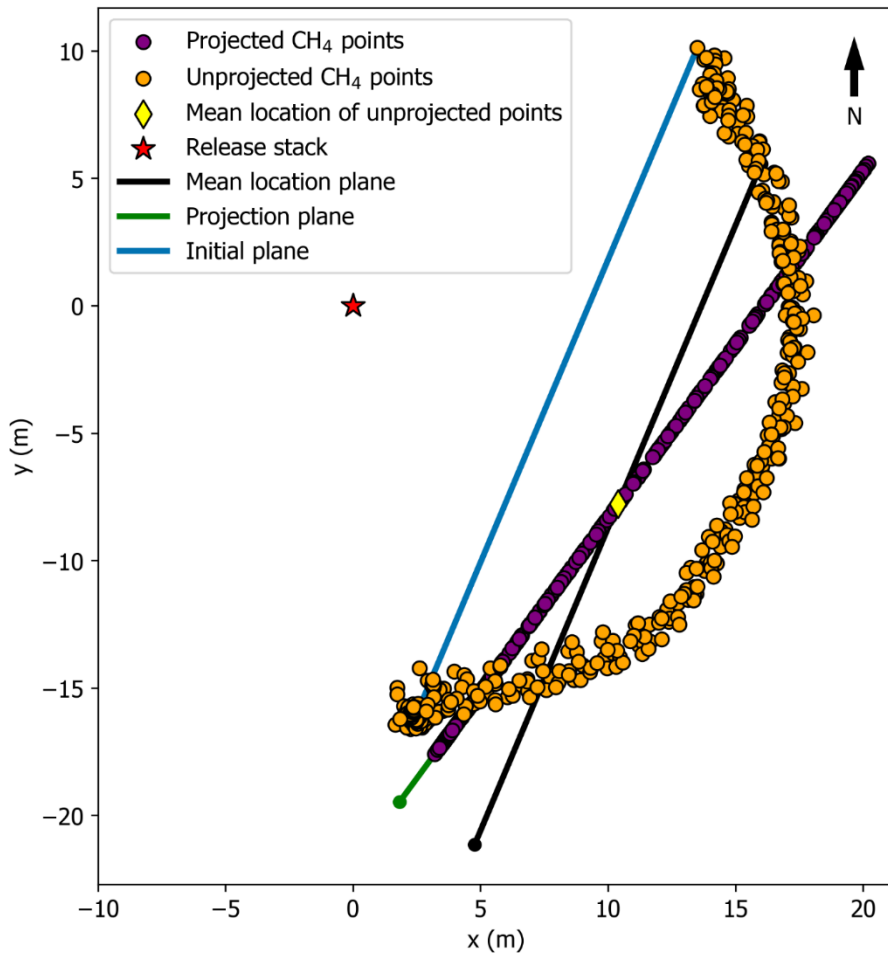
Figure 3. Flux plane definition and projection of CH₄ measurement points within a cartesian coordinate system for a 2.4 kg CH₄/h release on 12 June 2024 ~15m downwind. See the associated description of the procedure to define the flux plane and project the data in the text.

235

After defining and locating the flux plane, we projected the measurement points onto the plane (purple points Fig 3) using the dot product of the unprojected points (orange points Fig 3) and the plane. The line of projected data points was sometimes slightly shifted spatially on the plane that we defined depending on the spatial extent and angle of the plane relative to the 240 unprojected data points (Fig 3). Therefore, we used all projected data points and their spatial extent in our quantifications instead of only using projected points that fell within the bounds of our defined plane. Initially defining a slightly larger flux plane in the horizontal direction or addressing data density issues in calculating the plane's midpoint (yellow diamond Fig 3) would have mitigated this issue.

We then calculated the crosswind distances for each projected measurement point. The vertical extent of the flux

245   plane was set from 0 m (i.e., ground level) to the top measurement level plus half the distance between the top two measurement levels (Dooley et al., 2024). The total height of the plane was between 5m to 6.3 m depending on the experiment (Sect. 2.4.). The vertical extent of the plane was set to be larger than the range over which CH_4 mixing ratio was measured to extrapolate the lowest measurements down to the surface and the highest measurements slightly above the highest measurement height. This is an extrapolation of measured data, but helps ensure that each measurement is more equally weighted in the total flux

250   estimate.

We discretized the plane into a grid to estimate the CH_4 flux for each individual grid cell. The grid cell resolution was set to 0.5 m^2. This resolution was generally about one-half the vertical spacing of the CH_4 measurements, enabling interpolation of CH_4 between the different measurement heights. The rate estimates were not overly sensitive to changes to the grid cell resolution (2.9%, see S2 for a sensitivity analysis). Although, it should be noted that increasing the grid cell resolution beyond

255   the scale at which the measurements were collected (e.g., ~1m in this study) may result in oversmoothed interpolated plumes, artificially inflating the estimated rates. We used an Inverse Distance Weighted (IDW) squared method to interpolate measured data to the grid cell centers:

$$Z(P) = \frac{\sum_{i=1}^{n} \frac{Z_i}{d_i^2}}{\sum_{i=1}^{n} \frac{1}{d_i^2}} \tag{1}$$

260

where $Z(P)$ is the interpolated estimate of CH_4 mixing ratio at point P, Z_i is the measured CH_4 mixing ratio at a nearby point i, d_i is the distance in meters between interpolated point P and measured point i, and n is the number of measured points used to interpolate a value at $Z(P)$.

S3 explains our choice of IDW squared as the interpolation method. Figure 4a shows the interpolated CH_4 flux plane

265   for the 2.4 kg CH_4/h release on 12 June 2024 at 15 m downwind. It should be emphasized that Fig 4a is a spatially and temporally smoothed representation of the plume measured in this experiment, simulated with interpolation.
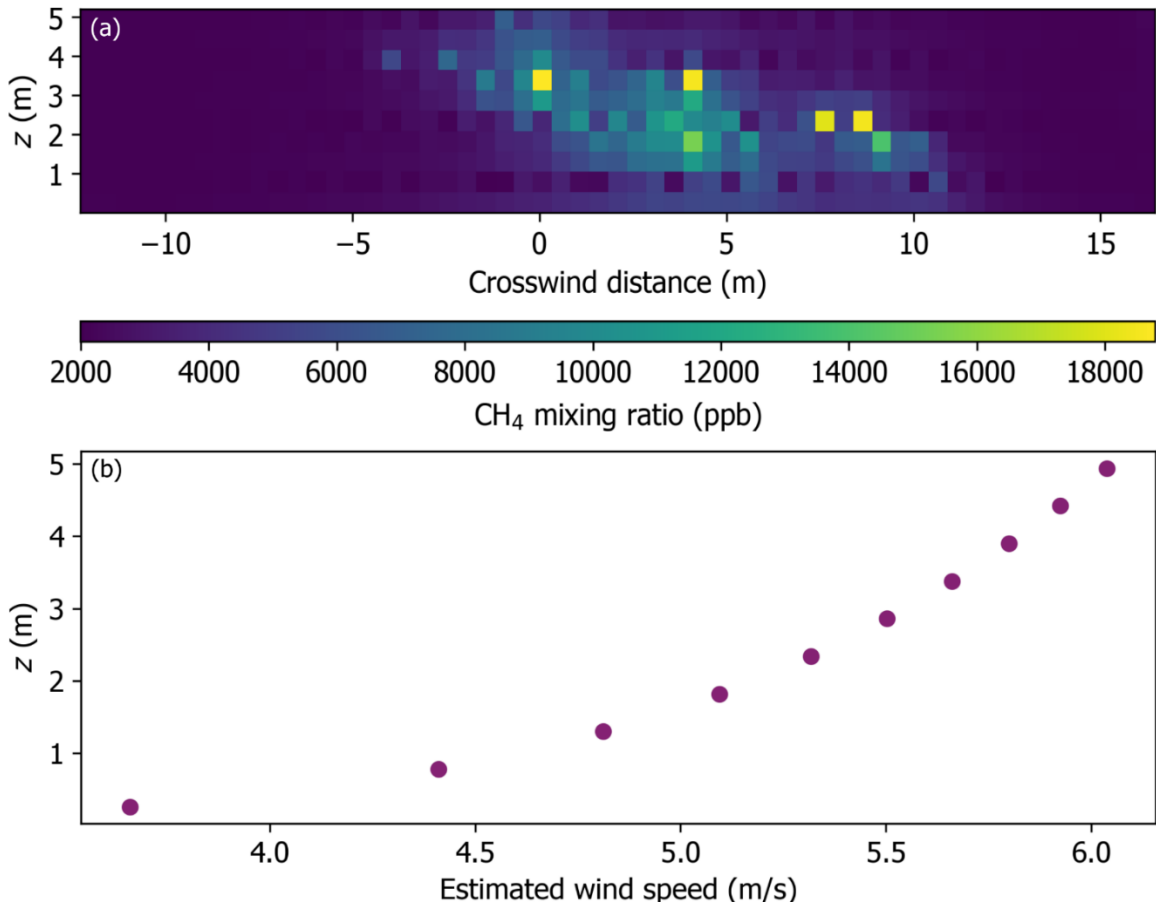
270

Figure 4. (a) Interpolated flux plane of CH₄ mixing ratios for the 2.4 kg CH₄/h release at 15m downwind distance on 12 June 2024, and (b) power law estimated vertical wind profile during the same experiment.

2.6.2 Vertical wind speed profile estimation

275   We measured wind speed at a height of 2.2 m during the experiments. As such, it was necessary to extrapolate the wind speed measured at this height to match the heights of the interpolated CH₄ mixing ratios for emissions quantification. A power law (Heier et al., 2014) was used to estimate wind speed for grid cell centers:

$$v_z = v_m \left(\frac{z}{z_m}\right)^a \tag{2}$$

280

where v_z is the unknown wind speed in m/s at height z, v_m is the mean wind speed in m/s measured during the experiments, z_m is the height at which wind speed was measured, z is the extrapolation height, and a is the wind shear coefficient.

For v_m in Eq. (2), we used the mean wind speed measured during the release, aligned with recording time. Drift in the data logger clock relative to the iPhone was negligible (< 1s). The wind shear coefficient, a, was set to 0.17, which was empirically derived in similar controlled release testing (Rella et al., 2015). More discussion of a is provided in S4, although S2 shows a lack of sensitivity of the quantified rates to different values of a. See Fig 4b for visualization of wind profile.

2.6.3 Flux plane quantification

After interpolating CH$_4$ mixing ratios onto the grid and estimating wind speed for the grid cell centers, we estimated CH$_4$ emissions rates for the release experiments using:

$$Q = \iint w_{gc} \left(\frac{(ch4_{gc} - ch4_{bg})}{10^6} \right) \rho_{ch4} res_{gc} t \qquad (3)$$

where Q is a CH$_4$ emissions rate in kg/h, the integrals represent integration over the two dimensions of the interpolated CH$_4$ and grid, w_{gc} is the estimated wind speed for each grid cell center, $ch4_{gc}$ is individual CH$_4$ grid cells, $ch4_{bg}$ is background CH$_4$ mixing ratio during the experiments, ρ_{ch4} is the density of CH$_4$ estimated for the time of the experiments using the Ideal Gas Law, pressure and temperature data, and the molar mass of CH$_4$, res_{gc} is the resolution of a grid cell in m^2, and t is 3600s. We used the fifth percentile of CH$_4$ mixing ratio during the experiments for $ch4_{bg}$.

Hourly atmospheric tower measurements of pressure and temperature from Environment and Climate Change Canada (ECCC) for Brooks, AB were used to calculate ρ_{ch4} (World Meteorological Association (WMO) ID: 71457).

2.6.4 Quality assurance

We developed a quality assurance protocol to identify surveys that are unlikely to produce reasonable results. Quality assurance protocols are essential in application to provide unambiguous guidance for subsequent field application of the method.

First, we screened all experiments to confirm that the measured peak CH$_4$ mixing ratio was below the top measurement level. All 44 (100%) out of the 44 controlled release experiments passed this criterion. This criteria provides indication that the majority of the plume was sampled and was not higher than sampled data.

To evaluate the geometry of the experiment, and better understand whether measured data captured the entirety of the plume, we estimated a Pasquill-Gifford (PG) stability class at the time of the experiments using the U.S. EPA's Key to Solar Radiation Delta-T Method (EPA, 2000). This method requires using 10 m wind speed, solar radiation, and time of day to look up a PG stability class from a table. We estimated the 10 m wind speed using the approach outlined in Sect. 2.6.2. and retrieved estimated solar radiation for the location and time of the experiments from NASA's POWER Project data access viewer (NASA, 2025). We used the estimated stability class and the downwind distance of the measurements to calculate a vertical dispersion parameter, σ_z, for each experiment using the Briggs-McElroy-Pooler Stability Class Lookup Table (Briggs, 1973). For each experiment, we examined the CH$_4$ time series and recorded the height at which we measured the highest CH$_4$

mixing ratio. We used this to approximate the vertical location of the plume's centerline. We then added this height to the calculated σ_z for that experiment and subtracted this value from the topmost measurement level, to estimate if the measurement plane captured the majority of the CH$_4$ plume. Negative values suggest that the highest measurement height may not have captured the full plume. This flagged 4 (9.1%) of the 44 experiments.

Third, we visually inspected the experiments flagged by the second criterion to determine if the measurements captured the majority of the plume. We inspected the data for (i) a discrete plume in the data centered around the peak CH$_4$ mixing ratio, and (ii) a decreasing trend in CH$_4$ enhancements with height, such that enhancements measured at the top height were less than one-half of the peak CH$_4$ enhancement. This signals that the majority of the plume was captured within the plane. It may not be necessary to measure in fully clean air above the plume to yield accurate rate estimates. One (2.3%) of the 44 experiments did not meet this criteria as CH$_4$ enhancements were less at the second-highest measurement level, then increased above one-half of the peak enhancement at the highest measurement level (see Fig S1 in S5). This plume likely changed vertical location between measurement of the top two measurement heights. In this experiment, the mean wind speed was the lowest of all experiments across the three testing days (2.8 m/s), resulting in an estimated PG stability class of B. We did include this experiment in the dataset, but is separately discussed to help learn how these situations affect results (see S5).

2.7 Optimized forward Gaussian method

The flux plane method requires that the majority of the CH$_4$ plume be captured within the measurement plane to accurately estimate emissions rates. In cases where the pole is insufficiently high to capture the majority of the plume, other methods are required. To address these situations, we explored the use of forward Gaussian plume model optimization on the data. This follows efforts from other workers— Nathan et al. (2015) applied a highly nuanced forward Gaussian optimization to confirm CH$_4$ emissions rates from a natural gas compressor station quantified with a fixed wing UAV and the flux plane method.

To test the forward Gaussian optimization method, we removed data from the top two measurement levels in 43 of the 44 experiments to simulate a situation where the pole can only reach the plume's centerline. This is equivalent to a 30% to 42% reduction in measurement height depending on the day of the experiment and the vertical capabilities of the kit on that day (Sect. 2.4.) or using a pole of about ~3.2 m to characterize the CH$_4$ emissions released from the ~2.4 m stack. To estimate emissions with this method, the plume's centerline should be measured at the top measurement height or below, enabling optimization of the plume's vertical dispersion coefficient, σ_z, based on measurement of the plume's bottom half. As such, for one experiment, we only excluded data from the top measurement level because the measured peak CH$_4$ mixing ratio occurred at an altitude of 4 m.

Figure 5a shows the 2.4 kg CH$_4$/h release at 15 m downwind where the peak CH$_4$ mixing ratio was measured at an altitude of 3.2 m; removing the top two measurement levels in this experiment simulated a situation where only the bottom part of the plume was measured.
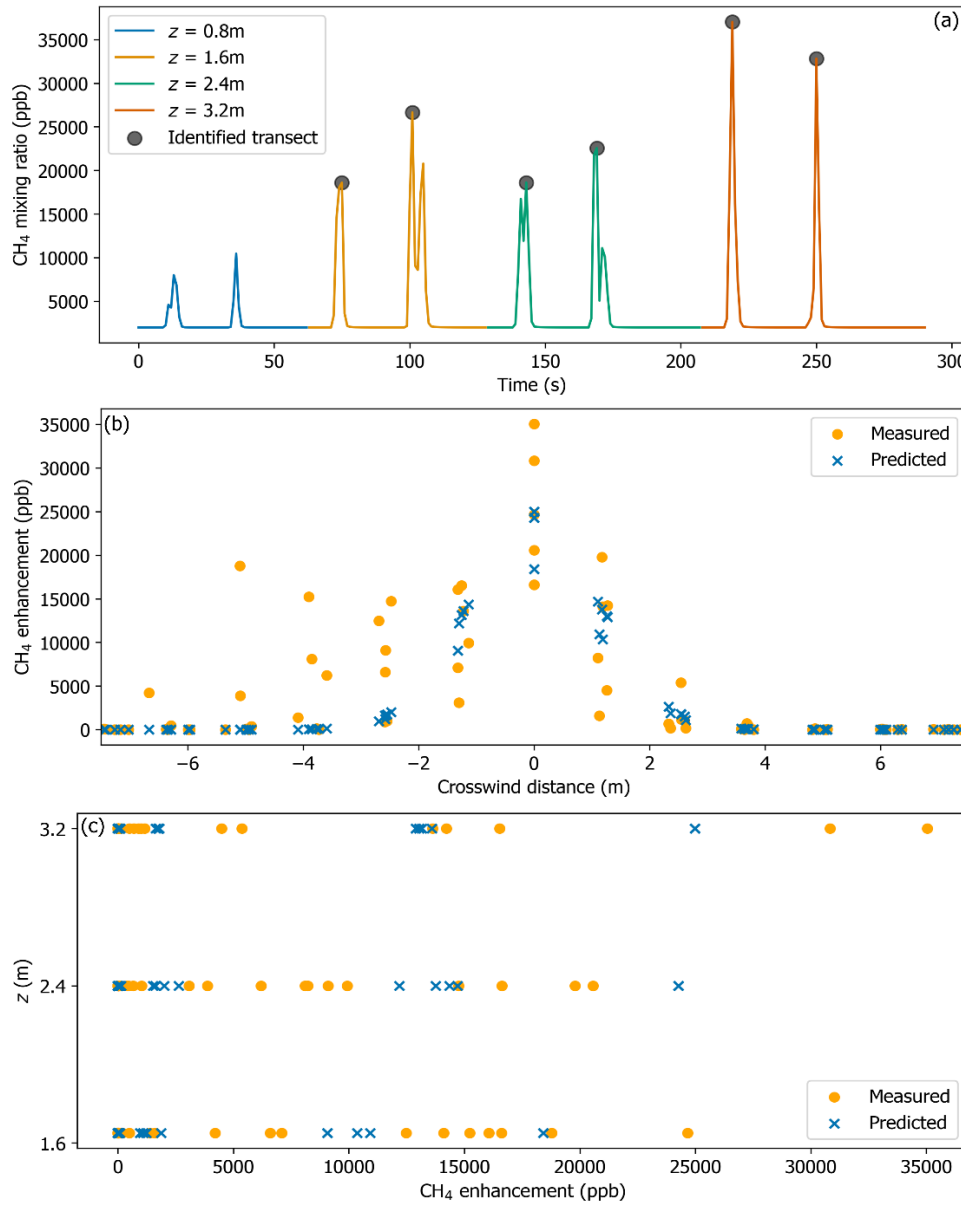
Figure 5. Experiment on 12 June 2024 at a release rate of 2.4 kg CH_4/h and 15 m downwind measurement distance. (a) transects by measurement height. The top two heights (4.0m and 4.8m) were removed to simulate a situation where the pole could only measure CH_4 at or slightly above the plume's centerline. Identified transects were selected for further data processing (see associated description in the text) and used in quantifying emissions. (b) and (c) horizontal and vertical fits of CH_4 mixing ratios predicted by the forward optimized Gaussian model to measured mixing ratios. The optimizer estimated a CH_4 emissions rate of 3.1 kg/h, which is equivalent to a 28.6% error relative to the release rate.

350

During algorithm development and testing, we noted a tendency of the forward Gaussian optimization method to substantially underestimate CH₄ emissions rates for some experiments when data from all measurement transects were used. We hypothesize this was due to the close-range nature of the measurements and their use within the optimizer. For the majority of release experiments—particularly when measurements were performed at very close downwind distances (e.g., 10m to 15m)—only a few walking transects had high CH₄ enhancements consistent with the vertical location of the plume's core, while others often had much lower enhancements. Given that the optimizer solved for the global minima between measured and predicted CH₄ mixing ratios based on Root Mean Square Error (RMSE), transects with low CH₄ enhancements dominated the optimizations when these were high in count, and predicted Gaussian plume peak concentrations were often much lower than measured. Thus, it was necessary to prioritize data from transects with high CH₄ enhancements to improve forward Gaussian model fits and rate estimates.

From test measurement heights, we identified transects with peak CH₄ mixing ratios that were greater than or equal to the sum of the mean CH₄ mixing ratio across all transects and two standard deviations (identified transects in Fig 5a) for further data processing. We found this criterion was optimal for estimating rates, as it targeted transects consistent with the plume's core vertically. We then sliced data from these transects centered around the transect peak (grey points in Fig 5a) and spatially aligned the plume centerlines of each transect following the approach described in S6. This corrected for changes in the wind direction across the transects that shifted the plume's location (Caulton et al., 2018). After alignment, we calculated the crosswind distance of the data points. The angle between the release stack and the location of the highest CH₄ concentration measurement across all identified transects served as the reference wind direction/plume's overall centerline (Sect. 2.6.1.) for the calculation.

We used a forward Gaussian plume model with ground reflection (Eq. 4) with an optimizer to minimize the RMSE between predicted and measured CH₄ mixing ratios. Eq. (4) describes the forward Gaussian plume model:

$$C(x,y,z) = \frac{Q}{2\pi\mu\sigma_y\sigma_z} exp\left(-\frac{y^2}{2\sigma_y^2}\right)\left[exp\left(-\frac{(z-H)^2}{2\sigma_z^2}\right) + exp\left(-\frac{(z+H)^2}{2\sigma_z^2}\right)\right] \tag{4}$$

where $C(x,y,z)$ is the CH₄ enhancement at location x, y, z predicted by the model, Q is the CH₄ emissions rate, μ is wind speed, σ_y and σ_z are the lateral and vertical plume dispersion coefficients, respectively, H is the effective stack height, and y and z are the crosswind and vertical distances from the centerline of the plume.

To optimize we used the Limited-memory Broyden-Fletcher-Goldfarb-Shanno method, with Box constraints (L-BFGS-B) to optimize the following parameters: Q, σ_y, σ_z, and H. The method allowed bounding of Q to prevent unrealistic rate estimates, which we set to 3.6 x 10⁻⁴ kg CH₄/h to 36 kg CH₄/h. Initial guesses were provided to the optimizer for Q, σ_y, σ_z, and H. We provided an initial value for Q at 3.6 kg/h. Other initial parameters, σ_y, σ_z, were estimated based on the Brigg's stability class at the time of the measurement (Sect. 2.6.4.). The initial value for H was the mean height of the identified transects in Fig 5a weighted by CH₄ mixing ratio. We bounded H in the optimizations to the initial value ± 0.5m, to minimize

potential fitting errors associated with plume meander vertically between the transects. Wind speed was estimated with the power law (see Sect. 2.6.2. for details) and we used this array of values for μ.

Predicted CH_4 mass densities from the Gaussian model were converted to mixing ratios. Figures 5b and 5c show the horizontal and vertical fits of the CH_4 mixing ratios predicted by the forward optimized Gaussian model to the measured mixing ratios for an experiment on 12 June 2024: release rate 2.4 kg CH_4/h and downwind measurement distance 15 m.

We evaluated the optimized values for Q, σ_y, σ_z, and H and the horizontal and vertical fits of the predicted CH_4 mixing ratios to the measured data to identify potential issues requiring intervention and explore the model's performance. The optimizer converged on a solution to minimize the scalar (objective) function 100% of the time but predicted unrealistic estimates for Q and σ_z in 3 (6.8%) of 44 experiments. This was evident by the prediction of very large values for σ_z that were one to two orders of magnitude larger than expected based on the estimated stability class at the time of the experiment. In these cases, we set σ_z to the optimized value for σ_y and re-ran the optimization. Poor estimates of σ_z by the optimizer were associated with experiments where plumes lacked a Gaussian shape in the vertical dimension, such those lacking a clear plume peak (e.g., high and similar CH_4 mixing ratios across the majority of transects then dropping sharply at higher altitudes), or those with notable meander of the plume's centerline. In one experiment the model predicted uniform concentrations across the test measurement heights, possibly due to the irregular plume structure measured in this experiment (see Fig S1). In this case we fixed H to the height at which the peak CH_4 mixing ratio was measured, improving the vertical fit.

3 Results

3.1 Testing envelope

Wind speeds across the 44 controlled release experiments on the 11, 12 of June and 6 of August 2024 averaged 4.8 m/s. Minimum wind speed was 2.8 m/s and maximum wind speed was 7.9 m/s (Fig 6a). Mean wind speeds were < 3 m/s in two (4.5%) out of the 44 individual experiments; wind speeds were generally between 4 m/s and 6 m/s in the majority of experiments. The experiments were performed over a wide range of temperatures (16.8 ºC to 29 ºC) with a mean of 22.9 ºC (Fig 6b). The lack of continuity of the data in Fig 6b reflects the different temperatures on each testing day. The 6 August 2024 had the lowest temperatures while the 11 June 2024 had the highest temperatures. The total number of experiments performed under the Briggs stability classes of B, C, and D were 2 (4.5%), 12 (27.3%), and 30 (68.2%), respectively. The mean survey time to complete the pole-based transects in the experiments was 9 min 35 s, varying from 6 min 20 s for closer downwind distances to 16 min 15 s for farther downwind distances (Fig 6c).
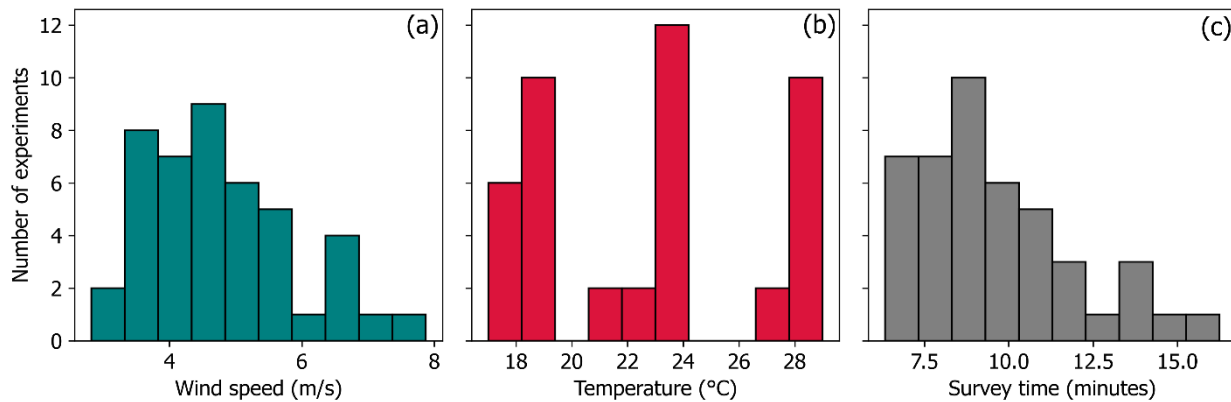
415

Figure 6. Envelope of testing conditions for controlled release experiments on 11, 12 of June and 6 of August 2024. (a) wind speed, (b) temperature, and (c) survey time. Temperature data was acquired from the ECCC weather station for Brooks, AB (WMO ID: 71457).

3.2 Flux plane quantification accuracy

We used Ordinary Least Squares regression in Python with a y-intercept of zero to compare estimated CH_4 emissions rates with the release rates. Figure 7 shows a fitted slope of 0.89 and an r^2 value of 0.96.
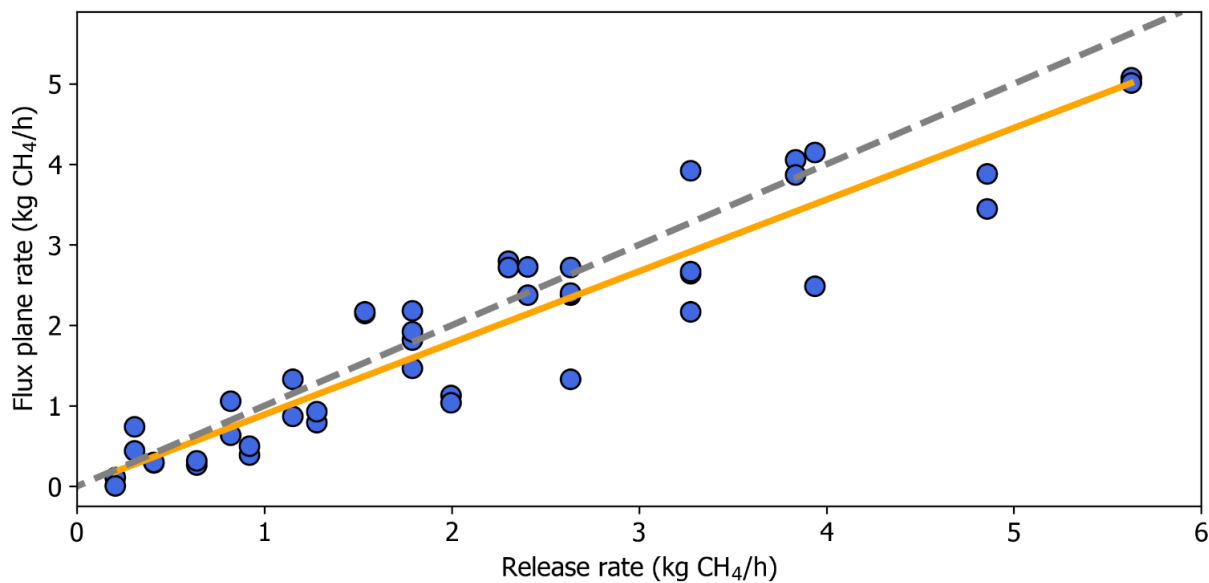
Figure 7. Ordinary Least Squares (OLS) regression of flux plane estimated CH_4 emissions rates on the release rates. The orange line shows the model fit and the grey dashed line is 1:1.

The mean percent relative error ((estimated rate – release rate) / release rate) * 100) of the CH_4 emissions rates estimated with the flux plane method was -10.1% (Fig 8a). Relative errors were mainly distributed around 0%, but a higher frequency of negative errors resulted in a left-skewed error distribution (Fig 8a), indicating a slight negative bias to the method. Approximately 68% of the quantified rates were within ±38.3% of the release rates. Minimum and maximum errors were - 97% and 141%, both of which were associated with experiments at the lowest (0.2 kg CH_4/h) and second lowest (0.3 kg CH_4/h) release rates, respectively.

Figures 8b to 8d generally show a lack of correlation between relative error and wind speed, release rate, and downwind distance. Figs 8b and 8c suggest (i) the flux plane method underestimated CH_4 emissions rates at higher wind speeds > 6 m/s, and (ii) larger errors were associated with lower release rates—errors decreased as the release rate increased. Figure 8d shows similar and fairly narrow error ranges within ±50% of the release rates across all downwind distances, although negative errors appeared more frequent at 10m downwind distance. More experiments are necessary to confirm these trends.
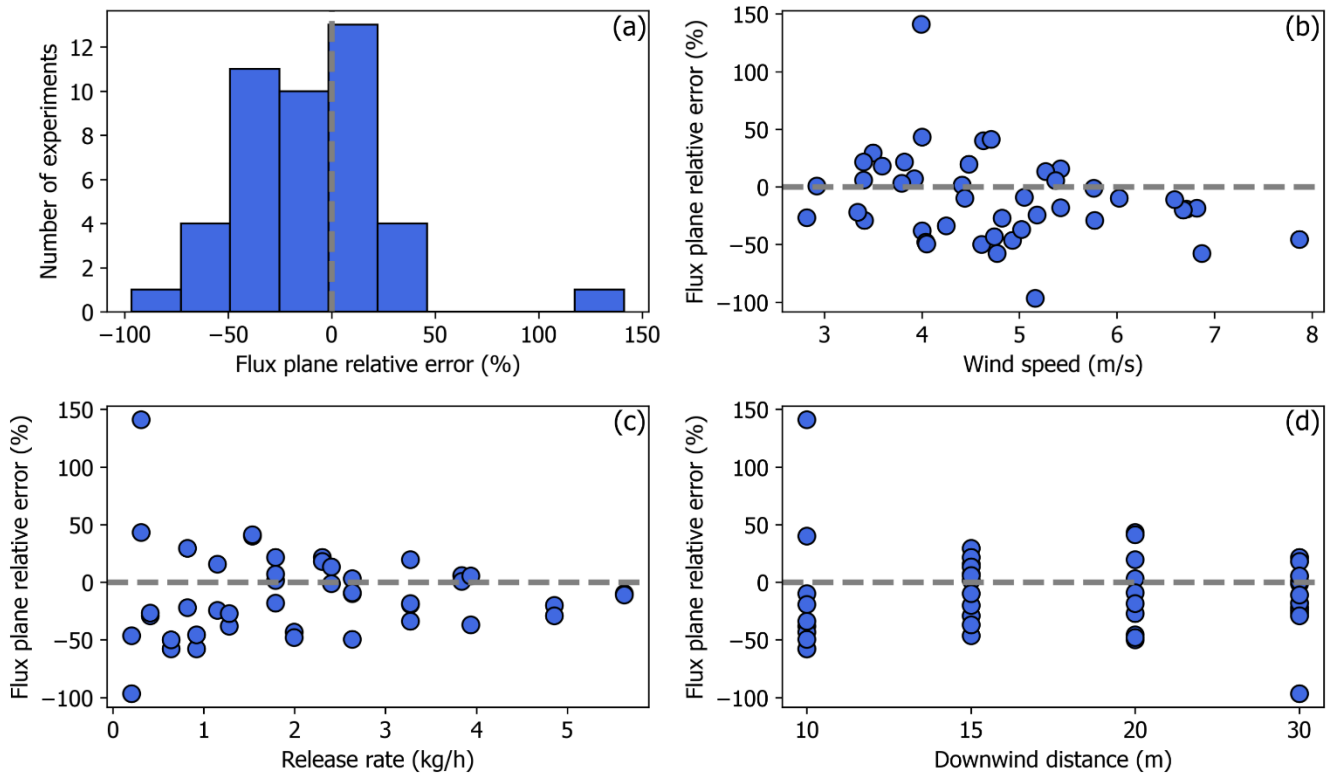
Figure 8. (a) Percent relative error distribution of the CH_4 release rates quantified with the flux plane method. (b), (c), and (d): percent relative error as a function of wind speed, release rate, and downwind measurement distance, respectively.

3.3 Forward Gaussian optimization quantification accuracy

To test the forward Gaussian optimization method, we removed the upper measurement heights (30% to 42% of the data depending on the experiment). Figure 9a shows the estimated CH_4 emissions rates with the forward Gaussian method (linear model slope = 0.97, r^2 = 0.92).

One data point deviated substantially from the 1:1 line in Fig 9a. This corresponded with a 4.9 kg CH_4/h release at a measurement distance of 30 m on 12 June 2024. We measured nearly identical peak CH_4 mixing ratios at 0.8 m and 4 m altitude during this experiment (see Fig S3). Based on the vertical distribution of CH_4 mixing ratios, the majority of the plume appeared to be located closer to the ground. When removing the upper measurement heights to test the forward Gaussian optimization method, the peak at 4m was removed. Given the deviation of this point from the 1:1 line, it is possible the irregular vertical shape of the plume and the removal of the peak at 4m was related to the underestimated CH_4 rate. The 0.3 kg CH_4/h release at 10 m downwind produced the highest relative error of the experiments with both the flux plane and forward Gaussian methods. Approximately 68% of estimates were within ±51.1% of the release rates. Errors ranged from -98.5% to 223%, which is similar to the flux plane method. Figure 9b shows a more even distribution of errors around 0% compared to the flux plane method and suggests little bias to the method (2.4% mean relative error). Figures 9c to 9e show that the lack of correlation between quantification error and wind speed, release rate, and downwind distance are generally very similar to the flux plane method. Figure 9e suggests that the Gaussian method may not underestimate CH_4 emissions rates at 10m downwind distance as frequently as the flux plane method.

460
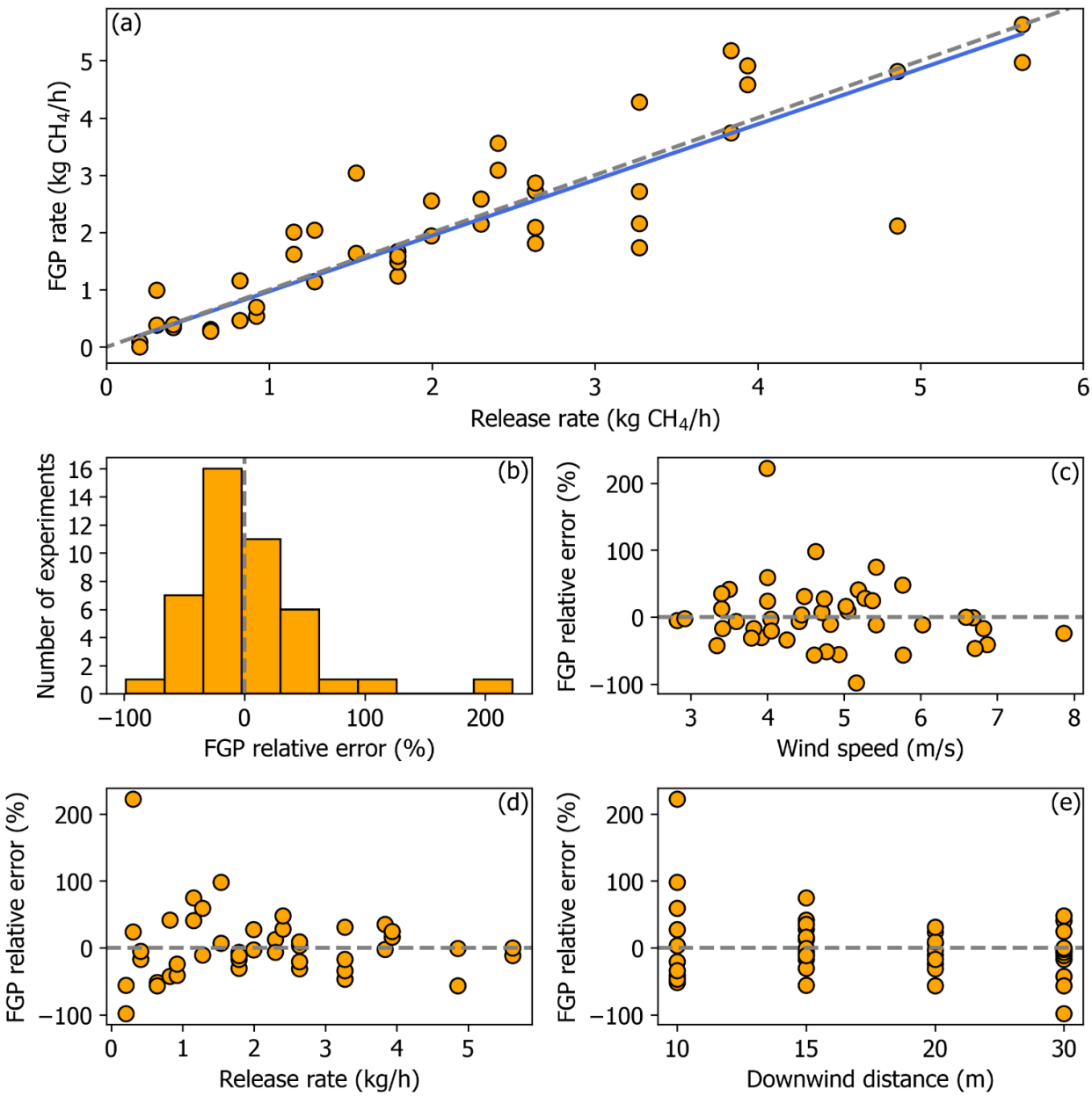
Figure 9. (a) Ordinary Least Squares (OLS) regression of optimized forward Gaussian plume (FGP) model estimated CH$_4$ emissions rates on the release rates. The blue line shows the model fit and the grey dashed line is 1:1. (b) percent relative error distribution of the CH$_4$ release rates quantified with the forward Gaussian optimization method. (c), (d), and (e): percent relative error as a function of wind speed, release rate, and downwind measurement distance, respectively.

465

Figure 10 shows that the CH₄ emissions rates quantified with the flux plane and the forward Gaussian methods are very similar despite removing the top two measurement levels from the latter for testing. Points do not deviate substantially from the 1:1 line. Forward Gaussian rates are generally larger, likely owing to the method's slight positive bias compared to the flux plane method's negative bias.
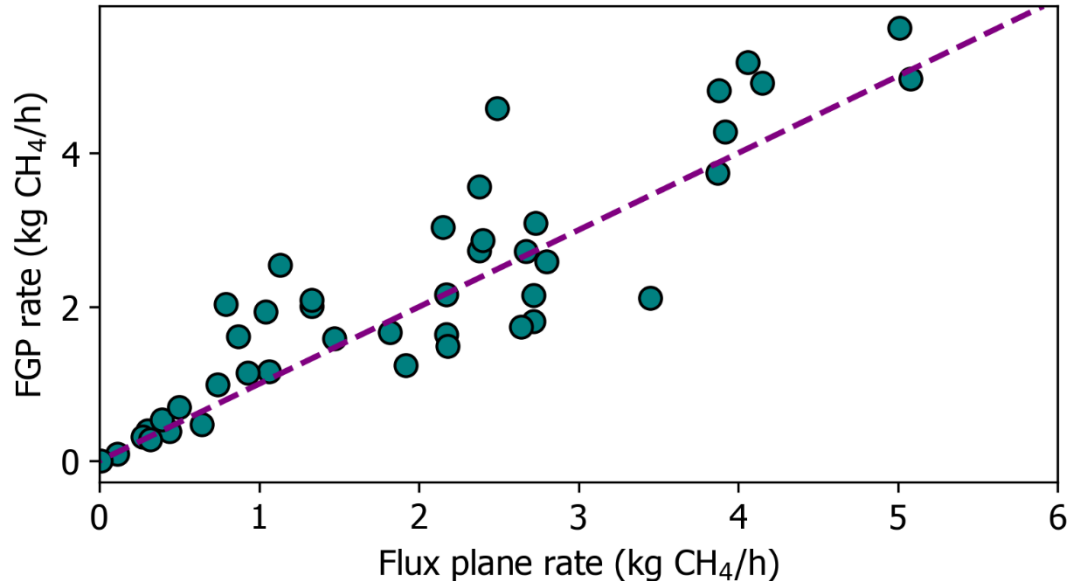
Figure 10. Comparison of CH₄ emissions rates quantified with the flux plane and forward Gaussian plume (FGP) optimization methods. All CH₄ measurement data was used with the flux plane method. The forward Gaussian method was tested by removing the top two measurement levels (30% to 42% of the vertical plume profiles) depending on the test day and vertical capabilities of the measurement kit on that day.

3.4 Replicate experiments

Some replicate releases were performed across different days for the rates 1.8 kg/h, 2.6 kg/h, and 3.3 kg/h. The initial releases were performed on 11, 12 of June 2024, the replicates were performed on 6 August 2024 at the same downwind distances. If all individual experiments at these rates are considered, percent relative errors ranged from -49.5% to 21.8% for the flux plane method (-46.8% to 30.8% for the forward Gaussian method). We grouped the initial and replicate experiments by release rate and downwind distance and averaged the mean relative error of the paired experiments. This constrained the range of relative errors from -29.6% to 4.5% for the flux plane method (-40.4% to 7.0% for the forward Gaussian method). Despite the limited number of replicate experiments performed, the results suggest that performing replicates can improve the accuracy of CH₄ emissions rate estimates.

4 Discussion

4.1 Testing representativeness

The results are linked to the characteristics of the controlled release setup, environmental conditions, the measurement kit, and specific downwind distances for data collection. We used a telescoping pole with vertical capabilities approximately 2 to 2.3 times the height of the release stack (~2.4 m) to measure CH_4 mixing ratios at close downwind distances (10 m to 30 m). CH_4 was released from the stack at approximately ambient temperature with low exit velocity, the latter of which was related to the stack diameter (3" to 4") and release rates. No obstructions that could have modified the turbulent mixing of CH_4 were present between the stack and the end of the telescoping pole. Nearly all experiments were performed in wind speeds ≥ 3m/s. Overall, plumes had minimal buoyancy upon exiting the stack, and results suggest that this situation was successful at capturing the full plume in the majority of cases.

To achieve reliable results with the human-portable pole method, a worker must have *a priori* knowledge of the source location(s), and ideally have some indications of the plume behaviour during the experiment. One of the primary limitations of the method is that there are physical constraints to the height of a pole that can be operated by a person. The pole used in this study could be improved. We estimate that the maximum vertical capability of a human-portable pole-based measurement kit, when hardware is sufficiently optimized, could be near 8 m. A pole with vertical capabilities of 8 m should fully capture most plumes (even with some plume buoyancy) from sources approximately one-half of this height ≤ 30 m downwind. To fully capture plumes from taller (e.g., 5 m to 6 m) or slightly buoyant plumes, measurements in higher wind speeds could be a solution to minimize plume rise. The rapid deployment and operational flexibility of the method means that it is logistically much simpler to be selective with measurement conditions, likely enhancing measurement quality. From our experiments, there is an upper wind speed limit. It is more challenging to stabilize the pole when wind speeds ≥ 7 m/s. This limit could be mitigated by using lower, more stable poles, with consideration of how this affects experiments and workers.

Applications for the human-portable pole method include quantifying CH_4 emissions from oil and gas wells and facilities with shorter (≤ 6 m) equipment under moderate to high wind speeds, individual short- to medium-height equipment under similar conditions, natural gas distribution and metering and regulating facilities, abandoned wells, some landfill gas capture infrastructure, shorter wastewater pumping and lift stations, compost piles, and likely many other sources at closer downwind distances. The pole method may not be practical or suitable for quantifying total CH_4 emissions from very large area sources such as landfills, wastewater treatment plants, or large cattle feed lots given the long distances required to fully transect plumes and the mismatch between the spatial scale of these sources and the height of the pole, which would result in limited characterization of plumes vertically. The methods demonstrated in this study could be used to quantify large area sources (e.g., Hossian et al., 2024) if paired with the measurement capabilities of quadrotor drones to substantially improve or ensure vertical plume capture. Site access may be required to execute pole-based measurements of some sources at closer distances, but other sources may be publicly accessible for measurement, monitoring, or independent confirmation (e.g., Hugenholtz et al., 2021). Shorter telescoping poles can be used to target shorter sources under appropriate conditions. The

pole-based iteration of the flux plane method is not an appropriate method to quantify CH_4 emissions from highly buoyant or lofted plumes due to stack exit velocity or temperature, such as compressor exhaust, high pressure line heater stacks without capped ends, or flare stacks. Drones provide a presently viable, but logistically more complex solution for these sources (e.g., Nathan et al., 2015).

4.2 Quantification accuracy

The human-portable flux plane method developed in this study using a telescoping pole to measure CH_4 emissions at close downwind distances estimated the release rates with a mean relative error of -10.1%. Approximately 68% of the estimated CH_4 emissions rates were within ±38.3% of the release rates.

One experiment deviated from the others (141% relative error), and examining the specifics of the release highlights important aspects of the method. For this experiment, CH_4 was released at the second-lowest rate of 0.3 kg/h, and measurements were taken at 10 m downwind. Figure S4 shows the CH_4 mixing ratio time series by measurement height. There was a prominent CH_4 peak of ~26 ppm measured at 3.2 m, which is almost double the second highest CH_4 measurement. This peak was measured during the second transect of the height. The peak CH_4 mixing ratio measured in the first transect was only ~3 ppm. The range of measured concentrations in this experiment signal that atmospheric dispersion was complex. There are several plausible dynamics. First, variable wind speeds at the source can result in variable concentrations downwind as the CH_4 is initially diluted into the atmosphere at the release stack. For example, a lull at the stack could have created a pocket of high CH_4 concentration—which was subsequently advected downwind. Second, mixing at these close ranges can be unpredictable—certain turbulence structures could maintain very high concentrations without lateral mixing. Third, the plume moves up and down with turbulent structures. Because measurement of each height was offset in time (c.f., Rella et al., 2015), each transect could intersect different parts of the plume. It is possible that subsequent transects could 'double count' the peak of the plume, or in other cases completely miss the center of the plume. Meaningful proxies for conditions where these types of dynamics exist could include wind speed or direction variability within the experiment. Future work could tightly sync co-located wind data to precisely identify the wind signatures associated with turbulent features, modeling their impact on the walking measurements. Further, measuring at further downwind positions (> 10 m) theoretically should reduce the strength of effects associated with variable near-source mixing. This effect is not strong, if it exists at all (Figure 8d), but may require further work to explore in more depth.

In general, there was a lack of correlation between percent relative error and wind speed, release rate, and downwind distance, indicating that the performance of the flux plane method was not systematically affected by variations in these variables during the experiments. Although, larger errors were associated with low release rates ≤ 0.3 kg CH_4/h, and negative errors were possibly more frequent at wind speeds > 6 m/s and downwind measurement distances of 10m. This phenomena of relatively constant error across the full range of release rates highlights a potential performance limitation of the method for quantifying sources emitting CH_4 at very low rates, as relative error would continue increasing as rates decrease.

The test results of the human-portable flux plane method are comparable to those reported by Corbett and Smith (2022) for their drone system, albeit with some differences between testing designs and test envelopes. Corbett and Smith (2022) performed 12 non-zero releases at generally much larger rates than our work (0 kg CH_4/h to 25 kg CH_4/h). CH_4 was measured mainly at 50 m or 300 m downwind of the release point. CH_4 sensor types (open path vs. closed path) and frequencies (10 Hz vs 1 Hz) were also different between Corbett and Smith (2022) and our work. We used the results for the non-zero rates reported in Corbett and Smith (2022) to calculate a mean relative error of 5.6%; 68% of the estimated CH_4 rates in their study were within ±36.7% of the release rates. In their study, CH_4 was released from a 56 m tall crane, which is different from our near-surface releases. This is noteworthy in that the experimental design in Corbett and Smith (2022) probably did not require extrapolating CH_4 mixing ratios measured at the lowest level with the drone to the ground and it is likely all CH_4 would have been captured in their flight path. Extrapolation down to the surface for quantification is required in many applications of the flux plane method, such as measuring CH_4 emissions from oil and gas sites with shorter equipment. Drones have a minimum flight altitude. The results of Corbett and Smith (2022) are representative of the method's application to tall stacks or lofted plumes, but not individual oil and gas well pads with shorter equipment where plumes reside closer to the surface. Additionally, Corbett and Smith (2022) did not test any non-zero release rates <1 kg/h, where enhancements will be lower and potentially become less accurately isolated from sensor noise. We performed a total of twelve experiments at CH_4 release rates between 0.2 kg/h to 0.92 kg/h, and our results indicated that larger errors were associated with low release rates. Despite the aforementioned differences, errors reported here are similar in magnitude to those reported by Corbett and Smith (2022).

The test results can also be compared with Rella et al. (2015)'s controlled release testing of the flux plane method using a vehicle-based system; however, there were differences in the method. The CH_4 data were collected in a vertically synchronous flux plane pattern using a mast affixed to a vehicle's front bumper and a gas sample storage manifold. Rella et al. (2015) fit a Gaussian model vertically to horizontally integrated CH_4 mixing ratios to extrapolate the relatively low measurement heights upwards. This noted, comparing our results to Rella et al. (2015)'s provides additional context to the human-portable flux plane variant developed and tested in our work. Rella et al. (2015) performed 120 controlled releases at rates between 0.43 kg CH_4/h to 2.14 kg CH_4/h. The vehicle transected the controlled plumes at 5 m to 81 m downwind distances (mean 34 m). The mean release height in the study was 2.2 m, similar to our release height of ~2.4 m. Mean wind speeds (3.6 m/s) were lower in Rella et al. (2015)'s controlled testing than ours (4.8 m/s). The reported accuracy in the study was 24%, and based on the geometric standard deviation, 67% of estimates were within a factor of 1.9 of the release rates. This translates to an uncertainty range of -47% to 90%, although it is not directly comparable to our uncertainties, as we used arithmetic rather than geometric measures of central tendency in assessing error.

The vehicle-based flux plane method—as demonstrated in Rella et al. (2015)—was also evaluated in a simulation study (Kumar et al., 2021), but overall, there are practical limitations to the heights of poles that can be affixed to vehicles and subsequently, the heights of sources that can be measured at further downwind distances with this method.

The oil and gas industry is an ideal setting to apply the human-portable flux plane method because of the need to understand source rates that are elevated and difficult to measure with other approaches (Vollrath et al., 2024). One potential

585 application of this method is site-scale emissions quantification, which has a wide variety of existing methods. Caulton et al. (2018) summarize uncertainty ranges from several mobile (Lan et al., 2015; Rella et al., 2015; Yacovitch et al., 2015) and stationary (Brantley et al., 2014; Foster-Wittig et al., 2015) vehicle-based studies. Mobile vehicle-based methods, which typically use atmospheric dispersion models to estimate CH_4 rates based on brief downwind plume passes, generally yield much higher uncertainties (50% to 350%) than stationary vehicle-based methods (25% to 60%), which involve parking the

590 vehicle downwind, collecting data for ~20 minutes, and fitting a dispersion model to the data. CH_4 is usually measured at a single height with these methods (c.f., Rella et al., 2015). The larger uncertainties for mobile vehicle-based methods are largely due to their reliance on brief plume snapshots, which may not represent time-averaged plume characteristics (Caulton et al., 2018). Our results suggest that the human portable pole method achieves performance somewhere in between stationary and mobile vehicle-based methods.

595 The human portable pole method complements vehicle-based and other mobile methods such as drones, aircraft, and satellites. In addition to elevated sources, the pole method can quantify sources emitting CH_4 at lower rates owing to its close-range capabilities. Low-emitting sources may evade detection from other methods depending on downwind measurement distances or detection limits. The pole method generally cannot sample as quickly as these other methods, but is useful for performing targeted, independent, and multi-temporal measurements of moderately elevated or low-emitting sources at a close

600 range. Sampling times are comparable to stationary vehicle-based methods (e.g., 20 minutes) but vary depending on the spatial extent of sources. Similar to the pole method, drones can be flown close to sources and thus measure low CH_4 rates. They also have a larger vertical measurement range and can access very tall sources such as $\geq$ 10 m tall tanks and flares which are unmeasurable with the pole method. This noted, the pole method is more accessible and practical than drones for measurements of a variety of CH_4 sources.

605 While we did not test CH_4 emissions rates representative of high emitting oil and gas sites in this study (e.g., 25 kg CH_4/h to 100 kg CH_4/h, Zavala-Araiza et al., 2018), the method's performance at the upper end of our tested range of release rates (0.2 kg CH_4/h to 5.6 kg CH_4/h) suggests that it could be used to reliably quantify higher emitting sources. Although, close-range measurements with the pole method at higher rates would likely result in CH_4 mixing ratios consistently exceeding the 0 ppm to 100 ppm measurement range of the LI-7810 trace gas analyzer used, which could introduce additional errors into

610 quantifications. There are also important health considerations for the pole operator if exposed to very high concentration plumes at a close-range, but operators could wear respirators or other personal protective equipment (PPE) to mitigate potential health effects in certain situations. The human portable pole method is best suited for quantifying moderately high sources and sources emitting CH_4 at generally lower rates, underscoring its complementarity to other mobile methods.

4.3 Forward Gaussian optimization method

615 We developed an alternative approach to quantify CH_4 emissions using data collected in the flux plane pattern in situations where measurements cannot fully capture the entirety of the plume. The experiments and calculations simulate using a telescoping pole that is slightly taller than the source and has a much higher chance of missing the upper portion of the plume.

This alternative approach achieved similar performance in estimating release rates compared to the flux plane method despite our removal of the top two measurement levels to test the method. The mean relative error across all estimates was 2.4% and 68% of estimates were within ±51.1% of the release rates, suggesting a slightly tighter error range and less bias compared to Rella et al. (2015)'s reported errors using a similar analytical method. Using optimization with constraints may have helped the Gaussian model successfully fit plume peaks in the vertical dimension despite temporal asynchrony to the measurement heights in this study and plume meander between the heights.

In some cases, CH_4 plumes as measured during the experiments did not closely conform to the Gaussian shape in the vertical dimension. Observed vertical plume shapes were often skewed with CH_4 mixing ratios falling rapidly at the second-highest or highest measurement heights. This depended on the downwind distance and wind speed during the experiments and the overall narrowness of plumes. Despite this, estimated rates with the forward Gaussian method were similar to the CH_4 release rates, demonstrating its efficacy as a method to use or fall back on in cases where the majority of a plume cannot be captured with the telescoping pole.

Removing the data acquired at the top two measurement levels during the experiments to test the forward Gaussian method simulated using a telescoping pole (~3.2 m) slightly taller than the source (~2.4 m) to measure CH_4. This simulated three scenarios: (i) the top measurement level aligned with the plume centerline, assuming some rise of the plume after exiting the stack; (ii) the top measurement level was slightly above the centerline, indicating the plume was sheared off the stack and allowing partial capture of its upper half; and (iii) in some cases, the plume was mixed downward, enabling full capture of the plume closer to the source despite the limited vertical extent of measurements. The tests and results encode each of these possible scenarios. CH_4 plumes are highly dynamic and thus it is nearly impossible to predict which of these three scenarios will happen when performing measurements. As a best practice when using this method, a measurement kit with vertical capabilities slightly taller (e.g., 1 m) than the source or the plume's predicted average location should be used. Infrared imaging of source plumes prior to measurements can support customizing a pole-based kit. Forward model results could improve if more vertical information on the plume's upper half is provided to the model, provided those measurements are made within the key mass of the plume and transects meet the criterion for further data processing used in this study. Overall, the method allows the height restrictions of the flux plane method to be slightly relaxed, increasing the height of sources that can be measured, such as slightly taller (~ 7 m) tanks or other taller oil and gas equipment.

We developed and tested the forward Gaussian optimization method based on a single-source release. Thus, the method, as documented in this study, should only be applied presently to single point-sources or smaller scale "point-sources" (e.g., oil and gas well pad) where potentially multiple co-located plumes are well mixed. Deviation from this risks applying the method in situations that poorly match the method's error characterization, and actual errors could be much greater. Oil and gas facilities with large spatial footprints and small distances between equipment groups should be avoided, as measurements at close distances would likely show several individual, poorly mixed plumes, which traditional Gaussian models cannot adequately reproduce (e.g., Nathan et al., 2015). Although, the single-source version of the Gaussian method could be used if individual plumes from a pole-based survey of a large oil and gas facility were spatially distinct enough to be

isolated. A multi-source inverse version of the Gaussian plume model has been used to successfully quantify CH_4 emissions from oil and gas production sites (Caulton et al., 2018). Future work may investigate the efficacy and performance of a multi-source configuration of the forward Gaussian optimization of pole-based measurements in estimating CH_4 emissions rates

655 from multiple sources at closer downwind distances.

4.4 Multiple measurements

Despite the limited number of replicate experiments performed, our results based on averaging errors suggest that performing multiple measurements improves the accuracy of CH_4 rate estimates. This aligns with findings from other recent studies that performed multiple plume transects in controlled release tests evaluating the quantification performance of mobile systems

660 (vehicles) for different applications (Barchyn et al., 2025; Tettenborn et al., 2025). More replicate experiments under a wider envelope of atmospheric conditions could further confirm the effect of multiple measurements in reducing error for the pole method. Overall, results from our replicate experiments indicate that measuring CH_4 emissions from sources multiple times under different conditions is valuable to improve the characterization of emissions and reduce uncertainties.

5 Conclusion

665 This study developed a new CH_4 emissions quantification method, adapting mass balance and forward Gaussian model methods to work with data measured with a human-portable pole. We tested the system in 44 individual controlled release experiments. We documented the methodology, addressing the overall poor reproducibility of the method presently based on a lack of details in the research literature. The human-portable flux plane method is a simple, accessible, and user-friendly variant of vehicle- and drone-based variants of the method for researchers. Moreover, the human portable variant has high

670 deployment readiness in that researchers can quickly mobilize when atmospheric conditions are optimal—this operational flexibility can yield better results.

The human-portable flux plane achieved a mean relative error of -10.1% in a series of 44 controlled release experiments with rates between 0.2 to 5.6 kg CH_4/h. A total of 68% of the quantified rates were within ±38.3% of the release rates, similar to the performance drone-based applications of the method (Corbett and Smith, 2022). There was a general lack

675 of correlation between relative error and wind speed, release rate, and downwind distance. Based on our results, we estimate that the method can be used to quantify CH_4 emissions from sources that are about one-half the height of the telescoping pole used under moderate wind and at closer downwind distances (≤ 30 m). Taller sources or slightly buoyant plumes from shorter sources can be targeted in periods of higher wind speeds owing to the method's high deployment readiness and operational flexibility.

680 There are physical limitations to the height of a telescoping pole that a person can reasonably operate. Therefore, the traditional flux plane method—where the majority of the CH_4 plume must advect through the plane—is not always appropriate depending on the source, downwind distance of the measurements, or atmospheric conditions. Thus, we developed and tested

an extension of the flux plane method based on forward Gaussian model optimization. The method extension uses data collected in the same pattern but is processed differently and designed to be used in cases where the traditional flux plane method cannot fully capture the plume vertically. We tested the method by removing the top two measurement heights from the forward Gaussian optimizations. The method was slightly less precise than the flux plane method and had less bias. The mean relative error was 2.4% and 68% of estimates were within ±51.1% of the release rates.

From this study, we recommend for the forward Gaussian method that (i) the telescoping pole must be sufficiently tall that it can measure the plume's centerline at minimum, and (ii) the spatial extent of sources such as oil and gas well pads is small enough that potentially separate plumes from different sources mix into a single "site level" plume before being transected downwind. At present, the forward Gaussian method documented in this study cannot quantify CH_4 emissions from large spatial extent, multi-plume sources. Future work may improve the Gaussian optimization algorithms developed as part of this study to handle multiple sources.

The human-portable flux plane method and its extension using forward Gaussian modeling is a new addition to the CH_4 emissions quantification toolkit designed to target moderate-height to slightly taller sources under moderate wind speeds and at closer downwind distances. The close-range capabilities of the pole method also enable measurements of sources emitting CH_4 at lower rates which may evade detection by vehicle-based systems, aircraft, and satellites depending on downwind measurement distances and detection limits. Many of the target sources for applying the pole-based flux plane and Gaussian methods are present in the oil and gas industry, but these methods can likely be applied to sources in other industries and sectors. The methods are accessible, reproducible, and rapidly deployable, which creates opportunity for researchers to independently measure, monitor, and confirm CH_4 emissions.

Data availability. The true release rates and the quantified CH_4 rates can be found at: https://doi.org/10.5683/SP3/BEQPG8

Author contribution. CH conceptualized the idea of using a pole to measure CH_4 mixing ratio at height. CV conceptualized using the flux plane method with a pole to quantify emissions. CV, CH, TB, AM, and CW designed and performed the controlled release experiments. CV developed the flux plane and forward Gaussian plume optimization algorithms and quantified the CH_4 emissions. CV analyzed the data and prepared a draft manuscript. All co-authors assisted in preparation of the final manuscript.

Competing interests. The authors declare they have no competing interests.

Acknowledgements. The authors would like to thank Joseph Samuel for his field assistance and Zhenyu Xing for providing a photograph of the controlled release setup.

Financial support. This project was undertaken with the financial support of the Government of Canada under the Calgary Urban Emissions Measurement Testbed project. Ce project a été réalisé avec l'appui financier du gouvernement du Canada. Additional financial support was provided by the Alberta Methane Emissions Program (www.amep.ca) and a doctoral scholarship from the Natural Sciences and Engineering Research Council (NSERC) of Canada.

References

Alvarez, R. A., Zavala-Araiza, D., Lyon, D. R., Allen, D. T., Barkley, Z. R., Brandt, A. R., Davis, K. J., Herndon, S. C., Jacob, D. J., Karion, A., Kort, E. A., Lamb, B. K., Lauvaux, T., Maasakkers, J. D., Marchese, A. J., Omara, M., Pacala, S. W., Peischl, J., Robinson, A. L., Shepson, P. B., Sweeney, C., Townsend-Small, A., Wofsy, S. C., and Hamburg, S. P.: Assessment of methane emissions from the U.S. oil and gas supply chain, Science, 361, 186–188, https://doi.org/10.1126/science.aar7204, 2018.

Barchyn, T., and Hugenholtz, C.: University of Calgary rapid vehicle-based methane emissions mapping system (PoMELO) single-blind testing results from the Methane Emissions Technology Evaluation Center (METEC), Harvard Dataverse [pre-print], https://doi.org/10.7910/DVN/BUT8GA, 2020.

Barchyn, T. and Hugenholtz, C.: Complex multi-source emissions quantification results for the PoMELO vehicle measurement system, test results from the CSU METEC facility, https://doi.org/10.31223/X5XP7B, 19 March 2022.

Barchyn, T., Hugenholtz, C. H., Myshak, S., and Bauer, J.: A UAV-based system for detecting natural gas leaks, J. Unmanned Veh. Sys., juvs-2017-0018, https://doi.org/10.1139/juvs-2017-0018, 2017.

Barchyn, T. E., Hugenholtz, C. H., and Fox, T. A.: Plume detection modeling of a drone-based natural gas leak detection system, Elementa: Science of the Anthropocene, 7, 41, https://doi.org/10.1525/elementa.379, 2019.

Barchyn, T., Clements, M., Gough, T., Hugenholtz, C., Munn, A., Samuel, J., Wearmouth, C., and Vollrath, C.: PoMELO Passive Blind Test Results: Emissions detection and quantification, https://doi.org/10.31223/X54Q65, 21 February 2025.

Brantley, H. L., Thoma, E. D., Squier, W. C., Guven, B. B., and Lyon, D.: Assessment of Methane Emissions from Oil and Gas Production Pads using Mobile Measurements, Environ. Sci. Technol., 48, 14508–14515, https://doi.org/10.1021/es503070q, 2014.

Briggs, G. A.: Diffusion estimation for small emissions. Atmospheric turbulence and diffusion laboratory, 965, 83-145, https://doi.org/10.2172/5118833, 1973.

Buchwitz, M., Schneising, O., Reuter, M., Heymann, J., Krautwurst, S., Bovensmann, H., Burrows, J. P., Boesch, H., Parker, R. J., Somkuti, P., Detmers, R. G., Hasekamp, O. P., Aben, I., Butz, A., Frankenberg, C., and Turner, A. J.: Satellite-derived methane hotspot emission estimates using a fast data-driven method, Atmos. Chem. Phys., 17, 5751–5774, https://doi.org/10.5194/acp-17-5751-2017, 2017.

Caulton, D. R., Li, Q., Bou-Zeid, E., Fitts, J. P., Golston, L. M., Pan, D., Lu, J., Lane, H. M., Buchholz, B., Guo, X., McSpiritt, J., Wendt, L., and Zondlo, M. A.: Quantifying uncertainties from mobile-laboratory-derived emissions of well pads using inverse Gaussian methods, Atmos. Chem. Phys., 18, 15145–15168, https://doi.org/10.5194/acp-18-15145-2018, 2018.

Conley, S., Franco, G., Faloona, I., Blake, D. R., Peischl, J., and Ryerson, T. B.: Methane emissions from the 2015 Aliso Canyon blowout in Los Angeles, CA, Science, 351, 1317–1320, https://doi.org/10.1126/science.aaf2348, 2016.

Conley, S., Faloona, I., Mehrotra, S., Suard, M., Lenschow, D. H., Sweeney, C., Herndon, S., Schwietzke, S., Pétron, G., Pifer, J., Kort, E. A., and Schnell, R.: Application of Gauss's theorem to quantify localized surface emissions from airborne measurements of wind and trace gases, Atmos. Meas. Tech., 10, 3345–3358, https://doi.org/10.5194/amt-10-3345-2017, 2017.

Corbett, A. and Smith, B.: A Study of a Miniature TDLAS System Onboard Two Unmanned Aircraft to Independently

750   Quantify Methane Emissions from Oil and Gas Production Assets and Other Industrial Emitters, Atmosphere, 13, 804, https://doi.org/10.3390/atmos13050804, 2022.

Dooley, J. F., Minschwaner, K., Dubey, M. K., El Abbadi, S. H., Sherwin, E. D., Meyer, A. G., Follansbee, E., and Lee, J. E.: A new aerial approach for quantifying and attributing methane emissions: implementation and validation, Atmos. Meas. Tech., 17, 5091–5111, https://doi.org/10.5194/amt-17-5091-2024, 2024.

755   European Commission: Global Methane Pledge: From Moment to Momentum, https://energy.ec.europa.eu/system/files/2022-11/GMP%20COP27%20Joint%20Factsheet.pdf, 2022.

Foster-Wittig, T. A., Thoma, E. D., and Albertson, J. D.: Estimation of point source fugitive emission rates from a single sensor time series: A conditionally-sampled Gaussian plume reconstruction, Atmospheric Environment, 115, 101–109, https://doi.org/10.1016/j.atmosenv.2015.05.042, 2015.

760   Government of Canada: Regulations Amending the Regulations Respecting Reduction in the Release of Methane and Certain Volatile Organic Compounds (Upstream Oil and Gas Sector), https://www.gazette.gc.ca/rp-pr/p1/2023/2023-12-16/html/reg3-eng.html, 2023.

Heier, S.: Grid Integration of Wind Energy: Onshore and Offshore Conversion Systems, 1st ed., Wiley, https://doi.org/10.1002/9781118703274, 2014.

765   Hossian, R. I., Dudak, Y., Buntov, P., Canning, E., Martino, R., Fougère, C., Naseridoust, S., Bourlon, E., Lavoie, M., Khaleghi, A., Farjami, F., Ells, L., Berthiaume, M.-A., Hall, C., and Risk, D.: A Controlled Release Experiment for Investigating Methane Measurement Performance at Landfills, Final Report, FluxLab, St. Francis Xavier University, prepared for the Environmental Research and Education Foundation (EREF), 64 pp., 2024.

Howarth, R. W., Santoro, R., and Ingraffea, A.: Methane and the greenhouse-gas footprint of natural gas from shale formations:

770   A letter, Climatic Change, 106, 679–690, https://doi.org/10.1007/s10584-011-0061-5, 2011.

Hugenholtz, C. H., Vollrath, C., Gough, T., Wearmouth, C., Fox, T., Barchyn, T., and Billinghurst, C.: Methane emissions from above-ground natural gas distribution facilities in the urban environment: A fence line methodology and case study in Calgary, Alberta, Canada, Journal of the Air & Waste Management Association, 71, 1319–1332, https://doi.org/10.1080/10962247.2021.1942316, 2021.

775   Johnson, M. R., Tyner, D. R., Conley, S., Schwietzke, S., and Zavala-Araiza, D.: Comparisons of Airborne Measurements and Inventory Estimates of Methane Emissions in the Alberta Upstream Oil and Gas Sector, Environ. Sci. Technol., 51, 13008–13017, https://doi.org/10.1021/acs.est.7b03525, 2017.

Karion, A., Sweeney, C., Pétron, G., Frost, G., Michael Hardesty, R., Kofler, J., Miller, B. R., Newberger, T., Wolter, S., Banta, R., Brewer, A., Dlugokencky, E., Lang, P., Montzka, S. A., Schnell, R., Tans, P., Trainer, M., Zamora, R., and Conley,

780   S.: Methane emissions estimate from airborne measurements over a western United States natural gas field, Geophysical Research Letters, 40, 4393–4397, https://doi.org/10.1002/grl.50811, 2013.

Karion, A., Sweeney, C., Kort, E. A., Shepson, P. B., Brewer, A., Cambaliza, M., Conley, S. A., Davis, K., Deng, A., Hardesty, M., Herndon, S. C., Lauvaux, T., Lavoie, T., Lyon, D., Newberger, T., Pétron, G., Rella, C., Smith, M., Wolter, S., Yacovitch, T. I., and Tans, P.: Aircraft-Based Estimate of Total Methane Emissions from the Barnett Shale Region, Environ. Sci. Technol.,
785   49, 8124–8131, https://doi.org/10.1021/acs.est.5b00217, 2015.

Kumar, R., Mitchell, D. A., Steinhoff, D. F., Saide, P., Kosovic, B., Downey, N., Blewitt, D., and Monache, L. D.: Evaluating the Mobile Flux Plane (MFP) Method to Estimate Methane Emissions Using Large Eddy Simulations (LES), JGR Atmospheres, 126, e2020JD032663, https://doi.org/10.1029/2020JD032663, 2021.

Lamb, B. K., Edburg, S. L., Ferrara, T. W., Howard, T., Harrison, M. R., Kolb, C. E., Townsend-Small, A., Dyck, W., Possolo,
790   A., and Whetstone, J. R.: Direct Measurements Show Decreasing Methane Emissions from Natural Gas Local Distribution Systems in the United States, Environ. Sci. Technol., 49, 5161–5169, https://doi.org/10.1021/es505116p, 2015.

Lan, X., Talbot, R., Laine, P., and Torres, A.: Characterizing Fugitive Methane Emissions in the Barnett Shale Area Using a Mobile Laboratory, Environ. Sci. Technol., 49, 8139–8146, https://doi.org/10.1021/es5063055, 2015.

Lavoie, T. N., Shepson, P. B., Cambaliza, M. O. L., Stirm, B. H., Conley, S., Mehrotra, S., Faloona, I. C., and Lyon, D.:
795   Spatiotemporal Variability of Methane Emissions at Oil and Natural Gas Operations in the Eagle Ford Basin, Environ. Sci. Technol., 51, 8001–8009, https://doi.org/10.1021/acs.est.7b00814, 2017.

Li, H. Z., Seymour, S. P., MacKay, K., Wang, J. S., Warren, J., Guanter, L., Zavala-Araiza, D., Smith, M. L., and Xie, D.: Direct measurements of methane emissions from key facilities in Alberta's oil and gas supply chain, Science of The Total Environment, 912, 169645, https://doi.org/10.1016/j.scitotenv.2023.169645, 2024.

800   LI-COR: LI-7810 $CH_4/CO_2/H_2O$ Trace Gas Analyzer, https://www.licor.com/products/soil-flux/LI-7810, 2025.

Maazallahi, H., Stavropoulou, F., Sutanto, S. J., Steiner, M., Brunner, D., Mertens, M., Jöckel, P., Visschedijk, A., Denier Van Der Gon, H., Dellaert, S., Velandia Salinas, N., Schwietzke, S., Zavala-Araiza, D., Ghemulet, S., Pana, A., Ardelean, M., Corbu, M., Calcan, A., Conley, S. A., Smith, M. L., and Röckmann, T.: Airborne in situ quantification of methane emissions from oil and gas production in Romania, Atmos. Chem. Phys., 25, 1497–1511, https://doi.org/10.5194/acp-25-1497-2025,
805   2025.

Mohammadloo, T.H., Jones, M., van der Kerkhof, B., Dawson, K., Smith, B.J., Conley, S., Corbett, A., and IJzermans, R.: Quantitative estimate of several sources of uncertainty in drone-based methane emission measurements, Atmos. Meas. Tech., 18, 1301-1324, https://doi.org/10.5194/amt-18-1301-2025, 2025.

NASA: The POWER Project, https://power.larc.nasa.gov/, 2025.

810   Nathan, B. J., Golston, L. M., O'Brien, A. S., Ross, K., Harrison, W. A., Tao, L., Lary, D. J., Johnson, D. R., Covington, A. N., Clark, N. N., and Zondlo, M. A.: Near-Field Characterization of Methane Emission Variability from a Compressor Station Using a Model Aircraft, Environ. Sci. Technol., 49, 7896–7903, https://doi.org/10.1021/acs.est.5b00705, 2015.

Ocko, I. B., Sun, T., Shindell, D., Oppenheimer, M., Hristov, A. N., Pacala, S. W., Mauzerall, D. L., Xu, Y., and Hamburg, S. P.: Acting rapidly to deploy readily available methane mitigation measures by sector can immediately slow global warming, Environ. Res. Lett., 16, 054042, https://doi.org/10.1088/1748-9326/abf9c8, 2021.

Peischl, J., Eilerman, S. J., Neuman, J. A., Aikin, K. C., De Gouw, J., Gilman, J. B., Herndon, S. C., Nadkarni, R., Trainer, M., Warneke, C., and Ryerson, T. B.: Quantifying Methane and Ethane Emissions to the Atmosphere From Central and Western U.S. Oil and Natural Gas Production Regions, JGR Atmospheres, 123, 7725–7740, https://doi.org/10.1029/2018JD028622, 2018.

Ravikumar, A. P., Sreedhara, S., Wang, J., Englander, J., Roda-Stuart, D., Bell, C., Zimmerle, D., Lyon, D., Mogstad, I., Ratner, B., and Brandt, A. R.: Single-blind inter-comparison of methane detection technologies – results from the Stanford/EDF Mobile Monitoring Challenge, Elementa: Science of the Anthropocene, 7, 37, https://doi.org/10.1525/elementa.373, 2019.

Rella, C. W., Tsai, T. R., Botkin, C. G., Crosson, E. R., and Steele, D.: Measuring Emissions from Oil and Natural Gas Well Pads Using the Mobile Flux Plane Technique, Environ. Sci. Technol., 49, 4742–4748, https://doi.org/10.1021/acs.est.5b00099, 2015.

Schwietzke, S., Pétron, G., Conley, S., Pickering, C., Mielke-Maday, I., Dlugokencky, E. J., Tans, P. P., Vaughn, T., Bell, C., Zimmerle, D., Wolter, S., King, C. W., White, A. B., Coleman, T., Bianco, L., and Schnell, R. C.: Improved Mechanistic Understanding of Natural Gas Methane Emissions from Spatially Resolved Aircraft Measurements, Environ. Sci. Technol., 51, 7286–7294, https://doi.org/10.1021/acs.est.7b01810, 2017.

Tettenborn, J., Zavala-Araiza, D., Stroeken, D., Maazallahi, H., Van Der Veen, C., Hensen, A., Velzeboer, I., Van Den Bulk, P., Vogel, F., Gillespie, L., Ars, S., France, J., Lowry, D., Fisher, R., and Röckmann, T.: Improving consistency in methane emission quantification from the natural gas distribution systems across measurement devices, Atmos. Meas. Tech., 18, 3569–3584, https://doi.org/10.5194/amt-18-3569-2025, 2025.

Thoma, E., H. Brantley, B. Squier, J. Dewees, R. Segall, and R. Merrill.: Development of Mobile Measurement Method Series OTM 33, https://cfpub.epa.gov/si/si_public_file_download.cfm?p_download_id=528480&Lab=NRMRL, 2015.

Tullos, E. E., Stokes, S. N., Cardoso-Saldaña, F. J., Herndon, S. C., Smith, B. J., and Allen, D. T.: Use of Short Duration Measurements to Estimate Methane Emissions at Oil and Gas Production Sites, Environ. Sci. Technol. Lett., 8, 463–467, https://doi.org/10.1021/acs.estlett.1c00239, 2021.

U.S. Environmental Protection Agency (EPA): Meteorological Monitoring Guidance for Regulatory Modeling Applications. https://nepis.epa.gov/Exe/ZyPURL.cgi?Dockey=2000D6B8.TXT, 2000.

U.S. Environmental Protection Agency (EPA): EPA's Final Rule for Oil and Natural Gas Operations Will Sharply Reduce Methane and Other Harmful Pollution, https://www.epa.gov/controlling-air-pollution-oil-and-natural-gas-operations/epas-final-rule-oil-and-natural-gas, 2023.

Vollrath, C., Hugenholtz, C. H., and Barchyn, T. E.: Onshore methane emissions measurements from the oil and gas industry: a scoping review, Environ. Res. Commun., 6, 032001, https://doi.org/10.1088/2515-7620/ad3129, 2024.

Yacovitch, T. I., Herndon, S. C., Pétron, G., Kofler, J., Lyon, D., Zahniser, M. S., and Kolb, C. E.: Mobile Laboratory Observations of Methane Emissions in the Barnett Shale Region, Environ. Sci. Technol., 49, 7889–7895, https://doi.org/10.1021/es506352j, 2015.

850 Zavala-Araiza, D., Herndon, S. C., Roscioli, J. R., Yacovitch, T. I., Johnson, M. R., Tyner, D. R., Omara, M., and Knighton, B.: Methane emissions from oil and gas production sites in Alberta, Canada, Elementa: Science of the Anthropocene, 6, 27, https://doi.org/10.1525/elementa.284, 2018.

Zavala-Araiza, D., Omara, M., Gautam, R., Smith, M. L., Pandey, S., Aben, I., Almanza-Veloz, V., Conley, S., Houweling, S., Kort, E. A., Maasakkers, J. D., Molina, L. T., Pusuluri, A., Scarpelli, T., Schwietzke, S., Shen, L., Zavala, M., and Hamburg,

855 S. P.: A tale of two regions: methane emissions from oil and gas production in offshore/onshore Mexico, Environ. Res. Lett., 16, 024019, https://doi.org/10.1088/1748-9326/abceeb, 2021.

Zhang, Y., Gautam, R., Pandey, S., Omara, M., Maasakkers, J. D., Sadavarte, P., Lyon, D., Nesser, H., Sulprizio, M. P., Varon, D. J., Zhang, R., Houweling, S., Zavala-Araiza, D., Alvarez, R. A., Lorente, A., Hamburg, S. P., Aben, I., and Jacob, D. J.: Quantifying methane emissions from the largest oil-producing basin in the United States from space, Sci. Adv., 6, eaaz5120,

860 https://doi.org/10.1126/sciadv.aaz5120, 2020.